



UNIVERSITY OF LEEDS

This is a repository copy of *A Regime-Oriented Approach to Observationally Constraining Extratropical Shortwave Cloud Feedbacks*.

White Rose Research Online URL for this paper:
<https://eprints.whiterose.ac.uk/185996/>

Version: Published Version

Article:

McCoy, DT, Field, P orcid.org/0000-0001-8528-0088, Bodas-Salcedo, A et al. (2 more authors) (2020) A Regime-Oriented Approach to Observationally Constraining Extratropical Shortwave Cloud Feedbacks. *Journal of Climate*, 33 (23). pp. 9967-9983. ISSN 0894-8755

<https://doi.org/10.1175/jcli-d-19-0987.1>

© 2020 American Meteorological Society. Reproduced in accordance with the publisher's self-archiving policy.

Reuse

Items deposited in White Rose Research Online are protected by copyright, with all rights reserved unless indicated otherwise. They may be downloaded and/or printed for private study, or other acts as permitted by national copyright laws. The publisher or other rights holders may allow further reproduction and re-use of the full text version. This is indicated by the licence information on the White Rose Research Online record for the item.

Takedown

If you consider content in White Rose Research Online to be in breach of UK law, please notify us by emailing eprints@whiterose.ac.uk including the URL of the record and the reason for the withdrawal request.



eprints@whiterose.ac.uk
<https://eprints.whiterose.ac.uk/>

A Regime-Oriented Approach to Observationally Constraining Extratropical Shortwave Cloud Feedbacks

DANIEL T. MCCOY,^{a,b} PAUL FIELD,^{a,c} ALEJANDRO BODAS-SALCEDO,^c GREGORY S. ELSAESSER,^{d,e}
AND MARK D. ZELINKA^f

^a *Institute of Climate and Atmospheric Sciences, University of Leeds, Leeds, United Kingdom;* ^b *Department of Atmospheric Science, University of Wyoming, Laramie, Wyoming;* ^c *Met Office, Exeter, United Kingdom;* ^d *Department of Applied Physics and Applied Mathematics, Columbia University, New York, New York;* ^e *NASA Goddard Institute for Space Studies, New York, New York;* ^f *Cloud Processes Research and Modeling Group, Lawrence Livermore National Laboratory, Livermore, California*

(Manuscript received 24 December 2019, in final form 20 August 2020)


ABSTRACT: The extratropical shortwave (SW) cloud feedback is primarily due to increases in extratropical liquid cloud extent and optical depth. Here, we examine the response of extratropical (35°–75°) marine cloud liquid water path (LWP) to a uniform 4-K increase in sea surface temperature (SST) in global climate models (GCMs) from phase 5 of the Coupled Model Intercomparison Project (CMIP5) and variants of the HadGEM3-GC3.1 GCM. Compositing is used to partition data into periods inside and out of cyclones. The response of extratropical LWP to a uniform SST increase and associated atmospheric response varies substantially among GCMs, but the sensitivity of LWP to cloud controlling factors (CCFs) is qualitatively similar. When all other predictors are held constant, increasing moisture flux drives an increase in LWP. Increasing SST, holding all other predictors fixed, leads to a decrease in LWP. The combinations of these changes lead to LWP, and by extension reflected SW, increasing with warming in both hemispheres. Observations predict an increase in reflected SW over oceans of 0.8–1.6 W m⁻² per kelvin SST increase (35°–75°N) and 1.2–1.9 W m⁻² per kelvin SST increase (35°–75°S). This increase in reflected SW is mainly due to increased moisture convergence into cyclones because of increasing available moisture. The efficiency at which converging moisture is converted into precipitation determines the amount of liquid cloud. Thus, cyclone precipitation processes are critical to constraining extratropical cloud feedbacks.


KEYWORDS: Climate sensitivity; Cloud cover; Cloud microphysics; Cloud radiative effects; Clouds

1. Introduction

Our lack of ability to predict the change in shortwave (SW) radiation reflected to space by clouds in response to warming hobbles our predictions of future climate. Caldwell et al. (2016) demonstrated that uncertainty in this SW radiative cloud feedback on warming represented the largest contribution to uncertainty in climate sensitivity in phase 5 of the Coupled Model Intercomparison Project (CMIP5) generation of global climate models (GCMs) (Taylor et al. 2012). Model uncertainty in the SW cloud feedback is driven by differences in the representation of clouds in the planetary boundary layer, which strongly affect SW, but not longwave, radiation (Hartmann and Short 1980). The time and length scales of these clouds are much shorter than even the highest resolution simulation and must be parameterized. This leads to substantial disagreement in feedback from one model to another due to differences in parameterization.

The SW cloud feedback, while uncertain, does have features that manifest across GCMs. The most salient of these is positive feedback in the subtropics and negative feedback in the extratropics (Zelinka et al. 2012a,b, 2016, 2013). The manifestation of this dipole in cloud feedback in CMIP5 was found to be due to decreasing cloud coverage across the subtropics and extending into the extratropics (a positive feedback) and increasing cloud optical depth in the extratropics (a negative feedback) in response to warming (Zelinka et al. 2016). Analysis of observations (Clement et al. 2009; Klein et al. 1995; D. T. McCoy et al. 2017; Myers and Norris 2015, 2016; Norris et al. 2016; Qu et al. 2015) and large-eddy simulations (Blossey et al. 2013; Bretherton 2015; Bretherton and Blossey 2014; Bretherton et al. 2013; Rieck et al. 2012) support the positive subtropical SW cloud feedback predicted by GCMs (Klein et al. 2017). Support for a negative extratropical SW cloud feedback is less robust and it remains unclear what cloud processes are critical for driving it (Terai et al. 2019). Analysis of microwave observations of liquid water path (LWP; the vertically integrated mass of cloud liquid averaged across cloudy and clear skies) and cloud-top pressure (CTP) optical depth histograms by Ceppi et al. (2016b) in the context of GCM experiments supported a negative extratropical cloud feedback. Examination of long-term trends in microwave LWP and GCM LWP over the Southern Ocean shows enhanced LWP, consistent with a negative feedback in this region (Manaster et al. 2017). Regime-oriented analysis of microwave LWP and GCM LWP in extratropical cyclones shows enhancement in LWP with warming linked to enhanced moisture

 Denotes content that is immediately available upon publication as open access.

 Supplemental information related to this paper is available at the Journals Online website: <https://doi.org/10.1175/JCLI-D-19-0987.s1>.

Corresponding author: Daniel T. McCoy, dmccoy4@uwyo.edu

DOI: 10.1175/JCLI-D-19-0987.1

© 2020 American Meteorological Society. For information regarding reuse of this content and general copyright information, consult the AMS Copyright Policy (www.ametsoc.org/PUBSReuseLicenses).

convergence (McCoy et al. 2019). However, observations of cloud optical depth for boundary layer, liquid-topped clouds from spaceborne and surface remote sensing instruments show decreasing cloud optical depth with warming (Gordon and Klein 2014; Terai et al. 2016, 2019). This is consistent with Tan et al. (2019), which showed increased optical depth in cold clouds due to phase shifts and decreased optical depth in warm, liquid clouds in response to warming.

Weakened negative extratropical SW cloud feedback plays an important role in driving the higher climate sensitivity of GCMs participating in phase 6 of the Coupled Model Intercomparison Project (CMIP6) (Eyring et al. 2016) relative to CMIP5 (Taylor et al. 2012; Zelinka et al. 2020). Because of this, resolving the different conclusions from these lines of evidence is important. Here, we extend the regime-oriented analysis presented in McCoy et al. (2019) to include both cyclone and out-of-cyclone regimes and further consider an array of cloud controlling factors (CCFs) (Stevens and Brenguier 2009) utilized in previous studies (Myers and Norris 2015, 2016; Terai et al. 2016; Wall et al. 2017) that are empirically connected to LWP. As in Kelleher and Grise (2019) daily time-scale data are used to allow evaluation of CCFs within the context of midlatitude weather systems. The analysis carried out in the present study is directed at elucidating the processes that set the extratropical SW cloud feedback.

In section 2, we present the observations and GCM output used in this study, and the empirical analysis techniques utilized. In section 3, we show that present-day covariability between LWP and CCFs can predict the response of LWP to warming in a suite of GCMs. In section 3a, cyclone behavior is analyzed, and in section 3b all data outside of cyclones are analyzed. In section 3c, the response of extratropical LWP is linked to changes in reflected SW. In section 4, we summarize these results and provide suggestions for narrowing the feasible range of extratropical SW cloud feedbacks.

2. Methods

We examine extratropical variability for the period 1995–2005. The 1995–2005 period has been selected for study to overlap with both the period when reliable microwave observations exist (Elsaesser et al. 2017) and the AMIP period simulated in CMIP5. Only data over oceans are examined because microwave observations are not available over land. The latitude range defined as extratropical in this work is 35°–75°. This latitude band corresponds to the region of strong negative SW cloud feedback in GCMs (Zelinka et al. 2016).

In sections 2a and 2b, we detail the observations and the GCM output examined in this work. In section 2c, we describe the regime discrimination methodology. In section 2d, we give an overview of the analysis applied to in-cyclone and out-of-cyclone data in the remainder of this paper to constrain extratropical LWP changes.

a. Observations

LWP is aggregated from multiple satellite microwave sensors following the methodology of the multisensor advanced climatology of LWP (MAC-LWP; Elsaesser et al. 2017). LWP

is defined as an area mean and is thus a product of cloud extent and the amount of liquid in clouds. The definition of LWP is consistent with the output from GCMs. Retrieved LWP is largely insensitive to overlying ice cloud due to use of low-frequency microwave radiation in the retrievals (Elsaesser et al. 2017). The MAC-LWP algorithm partitions between precipitating and nonprecipitating liquid (Elsaesser et al. 2017). This partitioning approach has been shown to be consistent with convection-permitting simulations of cyclones where precipitation is frequent and heavy (McCoy et al. 2019). Outside of cyclones, McCoy et al. (2020) estimated that 7% of total liquid path is rain in the NH midlatitudes from GCM output. This small relative fraction of precipitation limits inaccuracy in the LWP partitioning by the MAC-LWP algorithm. In this study we only examine nonprecipitating liquid.

The meteorological state of the atmosphere is characterized using reanalysis from MERRA2 (Molod et al. 2015) and microwave observations of water vapor path (WVP) and 10-m wind speed (U_{10m}) from MAC-LWP. Observations of top-of-atmosphere shortwave fluxes from the CERES synoptic 1° (SYN1deg) dataset, edition 4 (Doelling et al. 2016, 2013; Wielicki et al. 1996), were used to characterize albedo. Mean solar insolation was calculated using the CERES EBAF-TOA edition 4 dataset (Loeb et al. 2009). As described in McCoy et al. (2018b), biases related to near horizon solar zenith angle (SZA) substantially affect albedo. As in McCoy et al. (2018b), albedo from CERES SYN1deg is calculated every three hours, and observations where SZA > 45° are removed in the calculation of daily mean albedo.

b. Global climate models

1) CFMIP2 MODELS

Phase 2 of the Cloud Feedback Model Intercomparison Project (CFMIP2) (Bony et al. 2011) models with available daily mean output suitable for performing this analysis were examined. These models are listed in Table 1. Atmosphere-only (AMIP) simulations using observed SST as a boundary condition are available for the period 1979–2008. These simulations were repeated with SST uniformly increased by 4 K and are referred to as AMIP + 4 K.

2) HADGEM3 DEVELOPMENT MODELS

In addition to examining the different GCMs participating in CFMIP2, we examine changes in cloud microphysical parameterizations between the Global Atmosphere 6 (GA6) and GA7.1 versions of the Met Office Unified Model (UM). UM GA7.1 is the version of the atmosphere model underpinning HadGEM3-GC3.1, which is the Hadley Center's contribution to CMIP6 (Walters et al. 2019). Bodas-Salcedo et al. (2019) performed simulations in the UM updating one piece of the model physics at a time to examine sensitivity to different structural changes in the UM. This suite of simulations gives us insight into the impact of changes in cloud microphysics. We examine the following models: GA6, GA6_MicOn, GA6AerMicErf_On, and GA7.1 (Table 1). GA6_MicOn corresponds to implementing the GA7.0 (not 7.1) changes to cloud microphysics and large-scale precipitation, in particular

TABLE 1. GCM simulations examined.

Model	Reference	Notes
CMIP5/CFMIP2		
HadGEM2-A	Collins et al. (2011); Martin et al. (2011)	
IPSL-CM5A-LR	Dufresne et al. (2013)	
IPSL-CM5B-LR	Hourdin et al. (2013)	
MIROC5	Watanabe et al. (2010)	
CNRM-CM5	Voldoire et al. (2013)	
HadGEM3-GC3.1 development models		
GA7.1	Bodas-Salcedo et al. (2019); Mulcahy et al. (2018)	The atmospheric model in HadGEM3-GC3.1
GA6AerMicErf_On	Bodas-Salcedo et al. (2019)	GA6_MicOn with the length scale over which turbulence mixes (mp_dz_scal) in the Furtado et al. (2016) mixed-phase cloud scheme doubled to agree with GA7.1
GA6_MicOn	Bodas-Salcedo et al. (2019)	GA6 with the turbulent mixed-phase scheme described in Furtado et al. (2016)
GA6	Bodas-Salcedo et al. (2019)	

implementation of a turbulence-based supercooled liquid water parameterization (Furtado et al. 2016). GA6AerMicErf_On corresponds to implementing changes to cloud microphysics, large-scale precipitation, aerosols, and the tuning to mixed-phase cloud mixing length scale factor as described in Mulcahy et al. (2018), bringing it fully into line with GA7.1. The changes to aerosol were found to have a minimal effect on cloud LWP (Bodas-Salcedo et al. 2019). Based on these experiments, we can examine the implementation of a new turbulence-based parameterization of supercooled liquid that substantially increases liquid cloud fraction (Furtado and Field 2017; Furtado et al. 2016) and the tuning of this parameterization for GA7.1.

c. Cyclone compositing

This work utilizes the Field and Wood (2007) cyclone compositing algorithm, which uses sea level pressure (SLP) to identify cyclone centers. Here we utilize the same compositing approach as applied in Bodas-Salcedo et al. (2014) to partition data into times when a cyclone center is within 2000 km (in cyclone) and when a cyclone center is 2000 km away (out of cyclone).

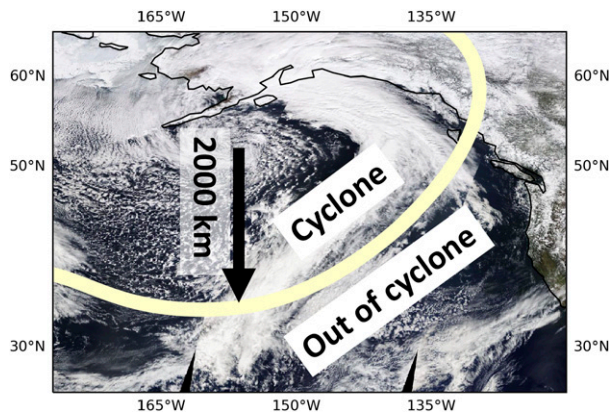


FIG. 1. An example of the cyclone compositing algorithm splitting data into cyclone and out-of-cyclone states.

An example partitioning is shown in Fig. 1. Data are regridded to a common $1^\circ \times 1^\circ$ spatial resolution before compositing.

The relative frequency of occurrence (RFO) of being inside or outside of a cyclone is calculated at each latitude and month of the year by calculating the ratio of $1^\circ \times 1^\circ$ grid cells inside and outside of cyclones. Observed RFO is used in all calculations in this work. (Cyclone RFO is shown in Fig. S1 in the online supplemental material.) Between AMIP and AMIP + 4K simulations storm tracks shift poleward (Fig. S1), but with substantial intermodel differences in the pattern of RFO changes. We assume a constant RFO for cyclones with warming. Changes in RFO between the AMIP and AMIP + 4K simulations were not found to meaningfully alter the results of this study. Comparison of AMIP + 4K and AMIPFuture simulations find that the response in circulation is fairly similar (Watt-Meyer et al. 2019). Based on this, it appears that the pattern of warming does not strongly affect the modeled circulation response.

d. Regression analysis

In this article we characterize the relationship between atmospheric state, so-called CCFs, and LWP in the present day using multiple linear regression. The ability of present-day variability to predict the response of clouds to warming is tested within the GCMs by examining how well the regression models trained in the present-day climate can predict the change in LWP between AMIP, and AMIP + 4K experiments.

The selection of predictor variables is based on previous work identifying CCFs (Myers and Norris 2016). The following CCFs are considered: SST (Myers and Norris 2016; Qu et al. 2015; Terai et al. 2016, 2019), estimated inversion strength (EIS) (Terai et al. 2016, 2019; Wood and Bretherton 2006), vertical pressure velocity at 500 hPa ω_{500} (Myers and Norris 2013), WVP, and wind speed at 10 m U_{10m} . The last two terms are combined to calculate a moisture advection term. This is discussed further below. Briefly, the mechanisms that are theorized to link clouds to each CCF are as follows: increased SST increases the efficiency of entrainment at cloud top (Bretherton and Blossey 2014), increased EIS reduces mixing across the inversion resulting in a moister boundary layer (Bretherton et al. 2013),

subsidence shallows the boundary layer (Blossey et al. 2013), and increased advection of moisture (here characterized as the product of U_{10m} and WVP) predicts increased precipitation rate (Field and Wood 2007; Harrold 1973). The product of WVP and U_{10m} has been shown to serve as a useful proxy for precipitation rate, the primary sink of cloud condensate in extratropical cyclones (Field and Wood 2007; Field et al. 2011; McCoy et al. 2018b; Pfahl and Sprenger 2016; Yettella and Kay 2017). Because cyclones dominate extratropical precipitation (Catto et al. 2012) controls on precipitation outside of cyclones have been less thoroughly studied. In the tropics WVP alone has been found to be a good predictor of precipitation rate (Bretherton et al. 2004; Gilmore 2015; Rushley et al. 2018). We analyzed the efficacy of $WVP \times U_{10m}$ and WVP alone in predicting precipitation rate in the CFMIP2 GCMs. It was found that, outside of cyclones, both $WVP \times U_{10m}$ and WVP predicted increased precipitation rate, but $WVP \times U_{10m}$ had a more uniform, monotonic relationship with precipitation rate and allows the use of a single predictor both inside and outside of cyclones. Thus, we use $WVP \times U_{10m}$ as a CCF both inside and outside of cyclones. The relationship between $WVP \times U_{10m}$ and precipitation rate is shown in Fig. S2. To maintain consistency with existing literature regarding cyclone precipitation $WVP \times U_{10m}$ is scaled by a constant [$c_{FW07} = 0.023 \text{ mm day}^{-1} \text{ m}^2 \text{ kg}^{-1} \text{ s m}^{-1}$] derived in Field and Wood (2007) when it is used as a CCF. Field and Wood (2007) calculated c_{FW07} from AMSR-E observations of cyclone-mean wind speed, WVP and rain rate. In cyclones we refer to $c_{FW07} \times WVP \times U_{10m}$ as warm conveyor belt moisture flux (WCB $\equiv c_{FW07} \times WVP \times U_{10m}$) to maintain consistency with previous literature. Outside of cyclones, $c_{FW07} \times WVP \times U_{10m}$ is written in full. Results of this study are qualitatively unchanged if WVP is used as the precipitation-related CCF rather than $c_{FW07} \times WVP \times U_{10m}$ outside of cyclones (not shown).

As discussed below, increases in WCB moisture flux and SST predict the majority of the LWP increase in the extratropics with warming. We will briefly discuss which components of WCB moisture flux change the most with warming in GCMs. Variation in U_{10m} and WVP both contribute to variability in cyclone WCB moisture flux in roughly equal proportion. Extratropical warming results in an increase in the WVP contribution to WCB moisture convergence, while U_{10m} stays approximately constant. The distribution of U_{10m} and WVP for the mean-state and warmed climate is shown in Fig. S3. Formulating CCFs combining U_{10m} and WVP to calculate WCB moisture flux means that the latent heat flux term is not characterized inside of cyclones. This has been found to affect the structure of extratropical cyclones (Hirata et al. 2016), but because U_{10m} is used in the calculation of WCB moisture convergence it is not used as a separate CCF. The inability of our analysis framework to separate contributions from latent heating in cyclones does not strongly affect our results based on tests of the time-scale invariance of the CCFs as shown in the remainder of the paper. One aspect of the projected LWP changes shown here is that the changes in some CCFs are more constrained than others. In particular, WCB moisture flux is the product of WVP and wind speed. The response of WVP to warming is strongly constrained by Clausius–Clapeyron, but

changes in U_{10m} are a function of changes in extratropical circulation and are less well constrained in GCMs. It is possible more advanced and higher-resolution models will project a different response in cyclone wind speed (Baker et al. 2019; Davini et al. 2017; Gonzalez et al. 2019; Jiayang et al. 2020; Roberts et al. 2020; Wu et al. 2019). However, across the GCMs evaluated here moisture changes dominate the change in WCB moisture flux.

We expect there to be a shift in LWP per degree increase in cloud temperature due either to changes in the slope of the moist adiabat (Betts and Harshvardhan 1987; Ceppi et al. 2017; Terai et al. 2019) or to deglaciation of cold clouds leading to a so-called mixed-phase cloud feedback on warming (Ceppi et al. 2016a; Kay et al. 2016; McCoy et al. 2015; Mitchell et al. 1989; Tan et al. 2016, 2019; Tsushima et al. 2006; Wall and Hartmann 2015). Because of this, we further partition our data inside and out of cyclones into regimes of SST to examine the behavior of warm and cold clouds separately. This is done by binning data into 2-K-wide SST regimes. In each SST bin, a regression model with the form

$$\text{LWP} = m_1 \text{SST} + m_2 \text{EIS} + m_3 \omega_{500} + m_4 c_{FW07} WVP \times U_{10m} \quad (1)$$

is trained. As noted above, to maintain consistency with the literature we will refer to the $c_{FW07} \times WVP \times U_{10m}$ term as WCB when discussing cyclones. Outside of cyclones the entire term $c_{FW07} \times WVP \times U_{10m}$ is written.

The regression model shown in Eq. (1) is trained on the present-day (AMIP) simulations and on observations, which are then used to predict the AMIP + 4K response in the models using the change in CCFs between AMIP and the AMIP + 4K simulations. The data within cyclones are averaged across individual cyclones (i.e., each daily mean cyclone 2000 km radius average becomes an individual data point in the regression). The data outside of cyclones are examined at $1^\circ \times 1^\circ$ resolution. All data are at daily mean resolution. Cyclone data are averaged together to create means for individual cyclones. This is done to enable the use of cyclone-mean predictors of precipitation rate in keeping with existing literature (Yettella and Kay 2017), as discussed above. Additional analysis of changes in structure within the cyclone system is provided in section 3a(3).

Regression models are trained on LWP and CCF data from each bin of SST in the AMIP simulations and observations. In the case of cyclone means, this bin corresponds to mean SST in the cyclone. Data from 35° to 75° in both hemispheres are used to train the regression model. This produces regression coefficients relating LWP to each CCF in each bin of SST.

3. Results

a. Inside of cyclones

1) CLOUD CONTROLLING FACTOR PREDICTION OF CHANGES IN LIQUID WATER PATH

Training the regression model shown in Eq. (1) on data from each GCM and on the observations reveals qualitatively consistent regression slopes between CCFs and LWP for observations and GCMs. Regression slopes in 2-K-wide bins of SST are shown in Fig. 2. LWP decreases with increasing SST

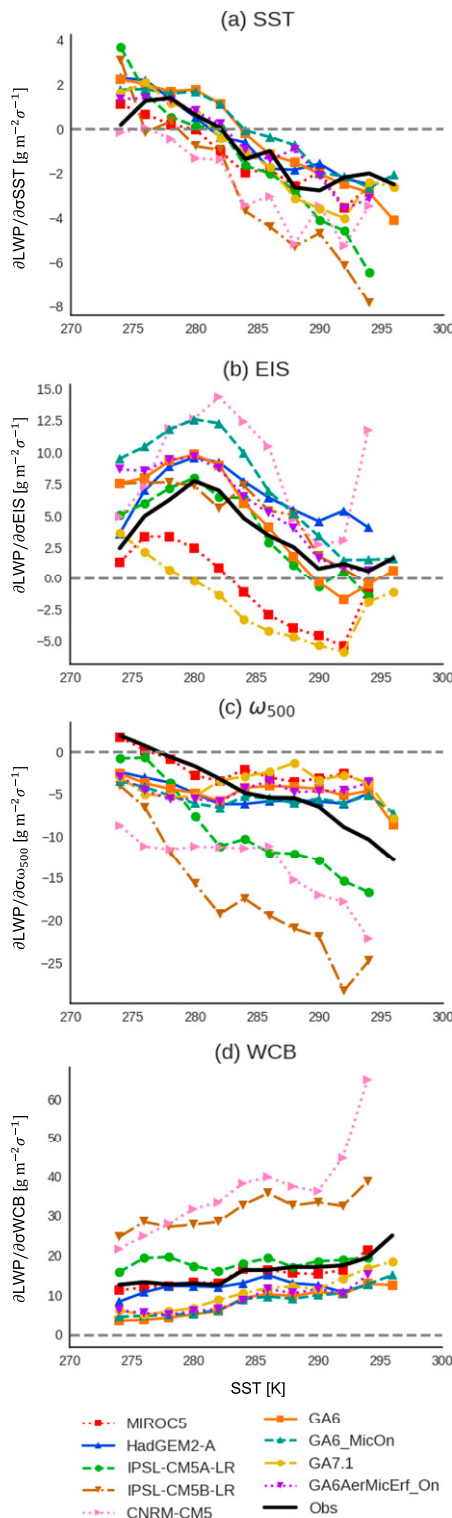


FIG. 2. Standardized multiple linear regression coefficients relating LWP to CCFs trained in 2-K-wide bins of SST for observations and GCMs using data from cyclones. The 95% confidence interval on observed regression coefficients is shown using black error bars but is generally too small to be visible. Dashed gray lines are shown at zero. Axis scales differ between subplots. Regression coefficients are normalized by the standard deviation of the CCF in each bin of SST. The same figure without normalizing the coefficients is shown in Fig. S4.

(Fig. 2a) except in the SST < 280 K regime. LWP increases with increasing EIS except in GA7.1 and MIROC5 (Fig. 2b). LWP decreases with increasing subsidence and increases with increasing WCB moisture flux (Figs. 2c,d). The regression slope relating CCFs to LWP exhibits dependence on the SST regime that the multiple linear regression model is trained in. This behavior can be seen in Fig. S4 where the regression slope unscaled by standard deviation in each SST bin is shown. This shows the absolute sensitivity to changes in a CCF and can be used to compared between bins of SST and across GCMs that have different standard deviations in CCFs—as opposed to the standardized sensitivities shown in Fig. 2, which can be used to compared between CCFs to see which contributes most strongly to variability in LWP.

GCMs and observations generally have a similar sensitivity of LWP to CCFs as a function of SST. The sensitivity of LWP to SST shifts from positive to negative as a function of increasing SST (Fig. S4a). The sensitivity of LWP to EIS peaks around 280 K (Fig. S4b), with the exception of MIROC5 and GA7.1. The sensitivity of LWP to ω_{500} becomes more negative as a function of SST (Fig. S4c), with the exception of the HadGEM3 model variants. The sensitivity of LWP to WCB moisture flux shows a slight decrease with increasing SST.

The observed relationship between LWP and CCFs falls roughly in the middle of the models and is consistent with previous studies (Klein et al. 2017; McCoy et al. 2019; Myers and Norris 2013). Because most previous studies focus on either changes in cloud extent or optical depth it is difficult to cleanly compare to the analysis of area-mean LWP (i.e., in-cloud LWP averaged over cloud and clear regions, see section 2a) presented here, as increased cloud extent or optical depth may increase area-mean LWP. Increased SST has been found to decrease cloud cover across the subtropics in observations and in large-eddy simulations (Klein et al. 2017). The occurrence of positive covariability between LWP and SST at low SST is consistent with the analysis presented in Terai et al. (2019), Tan et al. (2019), Ceppi et al. (2016b), and Tselioudis et al. (1992) that showed increased cloud optical depth in response to warming in cold clouds. Increased subsidence at a fixed EIS has been shown to decrease cloud cover, while EIS increases cloud cover at a fixed subsidence (Myers and Norris 2013). Increased WCB moisture flux has been shown to drive increased LWP in cyclones (McCoy et al. 2018b, 2019).

The response of LWP to a standard deviation in WCB moisture flux is large relative to other predictors (Fig. 2d). The mechanism underlying this relationship is driven by precipitation processes (McCoy et al. 2018b). WCB moisture flux is the primary source of moisture converging in cyclones and is matched by the precipitation sink in quasi-steady state (Field and Wood 2007; Field et al. 2008; McCoy et al. 2019) (Fig. S2). Cloud condensate acts as an intermediary state between moisture and precipitation. Therefore the efficiency with which cyclones can convert converged moisture to precipitation determines the slope relating WCB moisture flux to LWP. A schematic of this is shown in Fig. 3. Because WCB moisture flux is the product of WVP and U_{10m} this means that all else being held equal, WCB moisture flux will increase in a warmed climate following Clausius–Clapeyron. If a given GCM creates

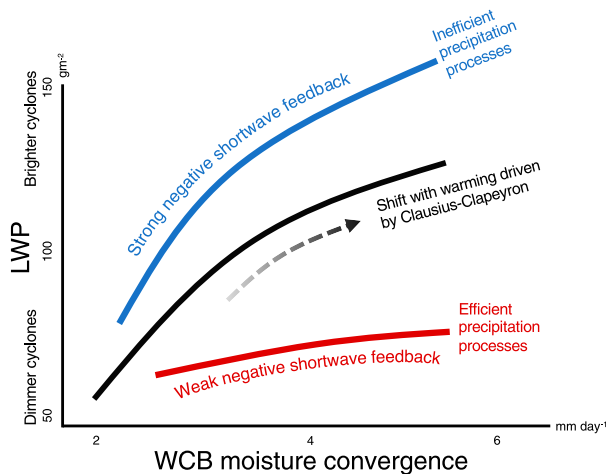


FIG. 3. A schematic illustration of the relationship between moisture convergence into cyclones, LWP, and shortwave feedback. Red and blue lines show hypothetical models with weak and strong negative extratropical cloud feedback due to high- and low-efficiency precipitation processes. The black line shows an intermediate precipitation efficiency case roughly consistent with observations. Approximate values of LWP and WCB moisture convergence are noted on the axis. The dashed line shows the direction of the shift in WCB moisture flux following a Clausius–Clapeyron-driven increase in WVP.

cyclones that are inefficient at converting converged moisture into precipitation, then it will have a strong relationship between LWP and WCB moisture flux, and by extension a more negative SW cloud feedback as discussed in section 3c. This mechanism is similar to the convective precipitation efficiency mechanism put forward in Zhao (2014). This was found to be a good predictor of GCM climate sensitivity across variants of the GFDL model by predicting changes in total condensate as a function convective precipitation efficiency (Zhao et al. 2016). The mechanism proposed here examines LWP, as opposed to total condensate. Measurements of ice water path are very uncertain (Jiang et al. 2012), but it appears that in convection permitting simulations cyclone ice water path does not vary with WCB moisture flux (McCoy et al. 2018b). Further examination of this weak dependence of ice amount on moisture convergence is needed in other high-resolution models that can accurately resolve frontal structures.

We have empirically related atmospheric state to LWP using multiple linear regression models (Fig. 2). Do these regression models have any utility in predicting the cloud response to a warming of the extratropics? To answer this question, we evaluate if the variability in the AMIP simulations can predict the change in LWP between AMIP and AMIP + 4 K. First, cyclone-mean quantities of each CCF are averaged to monthly means and $4^\circ \times 4^\circ$ latitude–longitude bins for the AMIP and AMIP + 4 K simulations. The sensitivity of LWP to each CCF is calculated from the regression model sensitivities (Fig. 2). Because the sensitivity of LWP to each CCF depends on SST

regime, as the climate warms the sensitivity of clouds to CCFs will be the average over the SST regimes in the mean state and warmed climates. That is to say, the sensitivity of LWP to CCFs in the SST bin corresponding to AMIP will not be representative to the sensitivity averaged over the SST regime between AMIP and AMIP + 4 K. To account for this, the sensitivity of LWP to CCFs is computed using the average of the sensitivity in the SST bin corresponding to AMIP and the sensitivity in the 4 K warmer SST bin for each latitude–longitude and month bin. To be clear, the sensitivities of LWP to CCFs are only computed from AMIP data. For each latitude–longitude bin, and monthly mean the sensitivity of LWP to CCF is multiplied by the change in each CCF between AMIP and AMIP + 4 K to yield a difference in LWP due to each CCF. The resulting predicted change in extratropical LWP in cyclones versus the change in LWP simulated by the GCM between AMIP and AMIP + 4 K simulations is shown in Fig. 4 for each GCM. The change in LWP between AMIP and AMIP + 4 K predicted by the regression models trained in the present agrees with the LWP change simulated by the GCMs. Examination of the contribution of each CCF in the regression model reveals that almost all the change in LWP between AMIP and AMIP + 4 K simulations is due to increasing SST (which tends to increase LWP at higher latitudes and decrease LWP at lower latitudes) and WCB moisture flux (which increases LWP at all latitudes) (Fig. 4). In turn, increased WCB moisture flux is almost entirely due to increased WVP (Fig. S3).

The predicted change in cyclone LWP between AMIP and AMIP + 4 K from observations is shown in Fig. 5 compared to the GCM prediction. The change in LWP is shown averaged across the 35° – 75° S and 35° – 75° N oceanic latitude bands and scaled by observed cyclone RFO as a function of latitude and month (Fig. S1). The observed mean-state RFO is used for all calculations due to it being interchangeable with the RFOs in the GCMs. By utilizing the regression model trained on observations (Fig. 2) and the change in CCFs between the AMIP and AMIP + 4 K simulations, we may predict an observational constraint on the response in LWP to uniformly increased SST.

The observational constraints for the NH and SH fall in the middle of the responses predicted by GCMs, with the change in LWP scaled by the observed RFO of cyclones predicted to be 2.7 – $4.0 \text{ g m}^{-2} \text{ K}^{-1}$ (SH) and 2.6 – $4.1 \text{ g m}^{-2} \text{ K}^{-1}$ (NH) (Fig. 5). The prediction is calculated using the sensitivity of LWP to CCFs derived from the observations, the change in CCFs in response to warming, and the skill of the regression model [Eq. (1)] in predicting the actual change in each GCM in response to warming. This corresponds to the intersection of the observationally inferred LWP change (vertical red and blue bars for the SH and NH, respectively) and the 95% confidence on the best fit line between the predictions of the multiple linear regression model for each GCM and the true response of each GCM (gray shading). The uncertainty range in the change in LWP predicted by the regression model trained on observations is from uncertainty in the change in CCFs as predicted by the GCMs. Uncertainties in the regression coefficients relating CCFs to LWP do not contribute significantly. The minimum and maximum uncertainty in change in LWP is shown as red

Change in LWP between AMIP and AMIP+4K as predicted by regression in cyclones

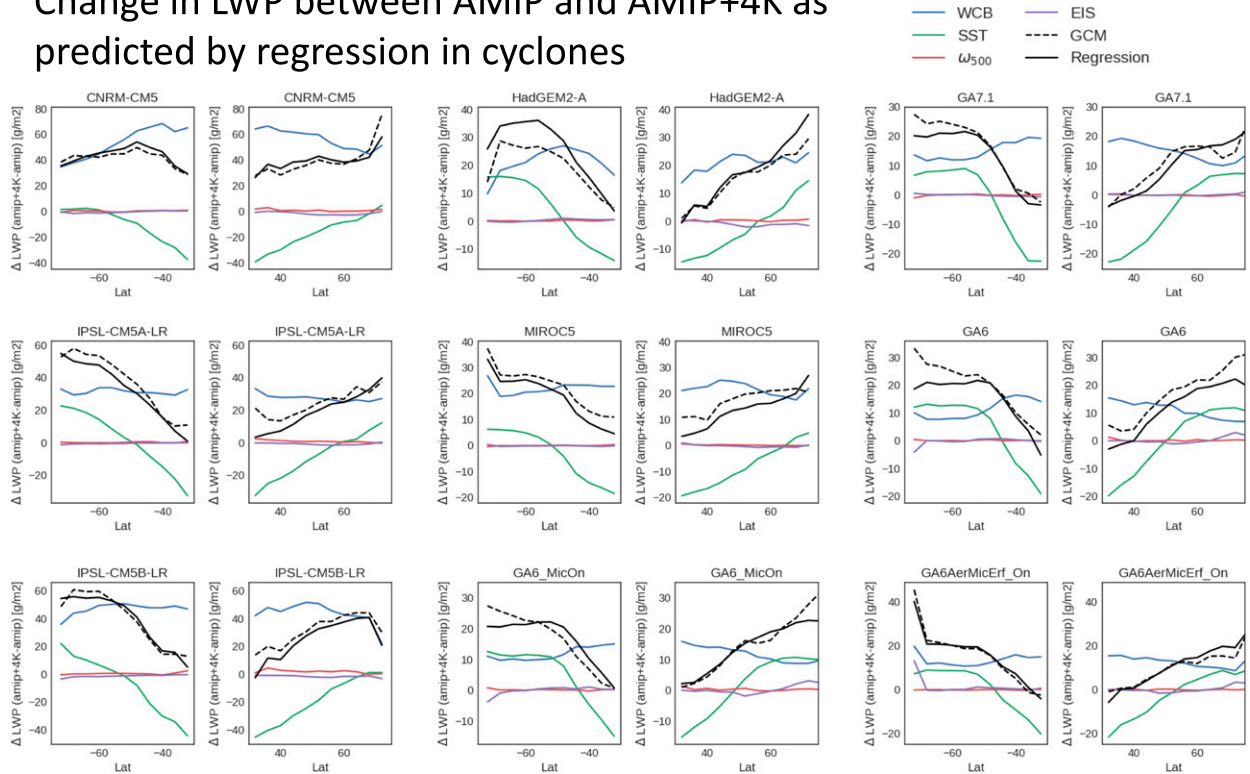


FIG. 4. The difference in cyclone LWP between AMIP and AMIP + 4 K simulations for each model considered in this study (dashed black line) and the prediction of the multiple linear regression model trained on the AMIP simulation (solid black line). Each hemisphere is shown separately. Individual predictor contributions to the change in LWP are shown for each model as noted in the legend. The change in LWP is not weighted by the relatively frequency of occurrence of cyclones.

and blue shading in Fig. 5 where distance on the x axis gives uncertainty.

2) EXPLORING PHYSICAL MECHANISMS IN HADGEM3 MODEL VARIANTS

In section 3a(1), we presented an empirical constraint on the change in extratropical cyclone LWP in a warming climate. This was done based on the sensitivity of LWP in cyclones to various CCFs. We will now examine what processes control this sensitivity. In particular, what factors might control the sensitivity of LWP to WCB moisture flux and SST, which we have found to dominate the LWP response to warming. One explanation of the extratropical enhancement in LWP with warming shown in models (McCoy et al. 2018a) and observations (Manaster et al. 2017) is deglaciation of mixed-phase clouds. Potential pathways include a simple repartitioning of ice and liquid, or a more complex reduction in precipitation efficiency following deglaciation (Ceppi et al. 2016a; Wall and Hartmann 2015). However, repartitioning of existing condensate underestimates the response of most models (Ceppi et al. 2016a; McCoy et al. 2015). This does not mean that model representation of cold clouds is unimportant to the extratropical LWP response. Ice hydrometeors act as an efficient sink of cloud liquid (Field and Heymsfield 2015).

If a given model creates ice at higher temperatures it is reasonable to expect that it will be more efficient at converting converged moisture into precipitation in cyclones and will have a lower sensitivity of LWP to WCB moisture flux (e.g., the red curve in Fig. 3). Structural differences between GCMs examined here makes it difficult to tie increasing sensitivity of LWP to WCB moisture flux to mixed-phase cloud representation. To analyze how mixed-phase clouds affect the sensitivity of LWP to WCB moisture flux and SST we turn to the HadGEM3-GA7.1 development models where different code packages were enabled one at a time. This allows us to definitively understand if changes in LWP are originating from changes to mixed-phase clouds and follows the causally aware techniques in Ceppi et al. (2016a).

Between GA6 and GA6_MicOn a new turbulent mixed-phase scheme that enhanced supercooled liquid water amount was added (Bodas-Salcedo et al. 2019; Furtado et al. 2016). This did not change $\partial\text{LWP}/\partial\text{SST}$ or $\partial\text{LWP}/\partial\text{WCB}$ appreciably (Figs. S4a,d). Between GA6_MicOn and GA6AerMicErf_On the scale factor in the mixing length of the new mixed-phase cloud scheme was doubled, further enhancing supercooled liquid (Furtado and Field 2017). The $\partial\text{LWP}/\partial\text{SST}$ and $\partial\text{LWP}/\partial\text{WCB}$ again remained relatively unchanged. Between GA6 and GA7.1 the aggregate of all model changes including

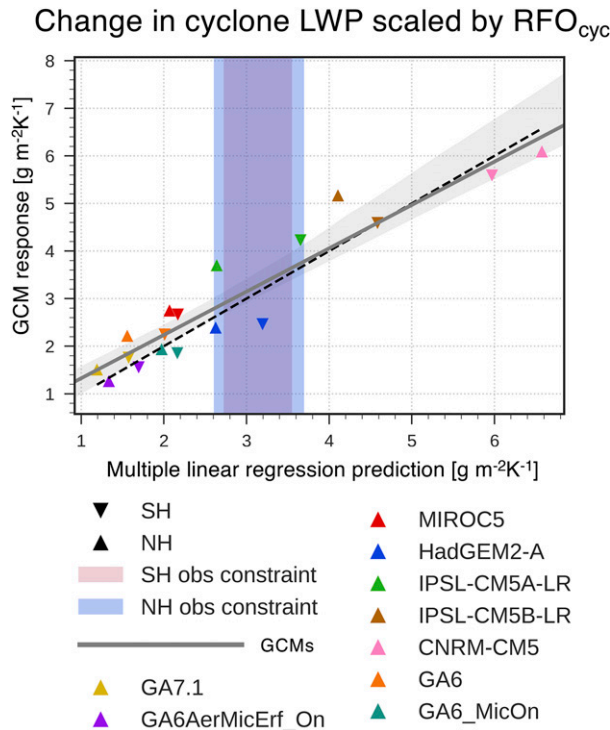


FIG. 5. GCM-predicted vs regression-model-predicted change in cyclone LWP between AMIP and AMIP + 4 K simulations over oceans in the 35°–75° latitude bands. Change in LWP is weighted by the observed RFO of cyclones. The best fit line and 95% confidence in the fit are shown in gray. The one-to-one line is shown with a dashed line. The change in LWP is normalized by 4 K. The observed sensitivity of LWP to CCFs is combined with the GCM-predicted change in CCFs to yield observational constraints for the NH and SH (shaded vertical bars). The minimum and maximum uncertainty in the change in CCFs across GCMs gives the width of the shaded areas.

changes to factors besides mixed-phase cloud was applied. This resulted in a slight increase in $\partial\text{LWP}/\partial\text{WCB}$. This lack of sensitivity to substantial changes in parameterization in the UM suggests that mixed-phase parameterization is not central in setting the efficiency at which cyclones convert converging moisture into precipitation across GCMs. Due to the complexity of implementing this experiment, our analysis is limited to one GCM and similar sensitivity studies in other GCMs are needed to confirm that this is not just a function of the two mixed-phase cloud parameterizations implemented in HadGEM3 that are studied here.

3) CHANGES IN CYCLONE LWP WITHIN CYCLONES

In sections 3a(1) and 3a(2), we examined changes in extratropical cyclones in the context of cyclone-mean behavior. This is advantageous because it allows us to leverage the synoptic-scale organization of these systems. Extending this analysis into evaluating changes in cyclone structure is not the goal of this paper, and this has been carefully examined elsewhere (Bodas-Salcedo 2018). The response of cloud structure within

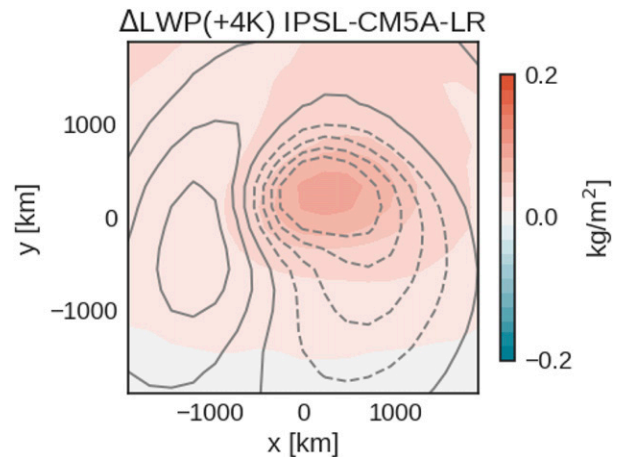


FIG. 6. Difference in LWP between AMIP and AMIP + 4 K simulations for IPSL-CM5A-LR. The equivalent figures for other GCMs are shown in Fig. S5. The difference in LWP is shown relative to cyclone centers. The y axis shows distance poleward from the low pressure center (SH cyclones are flipped in latitude to align with NH cyclones in the average). Contours of $\omega_{500\text{hPa}}$ are shown in gray. Dashed lines correspond to ascent and solid lines correspond to descent. Contours are equally spaced in intervals of 0.025 Pa s^{-1} .

cyclones to perturbations in the CCFs that we find to be central in setting the cyclone LWP response to warming is examined below.

For each GCM examined here we calculate the change in LWP relative to the cyclone center between AMIP and AMIP + 4 K simulations. LWP increases are generally on the poleward side of the cyclones and in the regions of large-scale ascent (an example from a GCM with an intermediate LWP response to warming is shown in Fig. 6, and remaining models are shown in Fig. S5). One exception is GA6 where increased LWP is centered in the post-cold frontal region. The shift in LWP increase location across GA6 variants (Fig. S5) suggests that while cyclone-mean $\partial\text{LWP}/\partial\text{WCB}$ may not be a strong function of mixed-phase processes in GCMs, the location of LWP response to warming may be. This supports the utility of performing similar tests of the mixed-phase parameterization in other GCMs.

How does the change in LWP shown in Fig. 6 and Fig. S5 relate to changes in the CCFs? To examine this, we use multiple linear regression to characterize the covariability between SST and WCB moisture flux and the LWP in cyclones. These predictors have been chosen because they were identified as the primary drivers of LWP change in the cyclone mean (Fig. 4). Example regression coefficients for the same model shown in Fig. 6 are shown in Fig. 7, and the regression coefficients for the remaining GCMs examined here are shown in Fig. S6. It is found that increased WCB moisture flux covaries with increasing LWP in regions of ascent. This is consistent with the precipitation efficiency argument put forward in Fig. 3. GCMs tend toward a higher $\partial\text{LWP}/\partial\text{WCB}$ than the observations (Fig. 2d). The

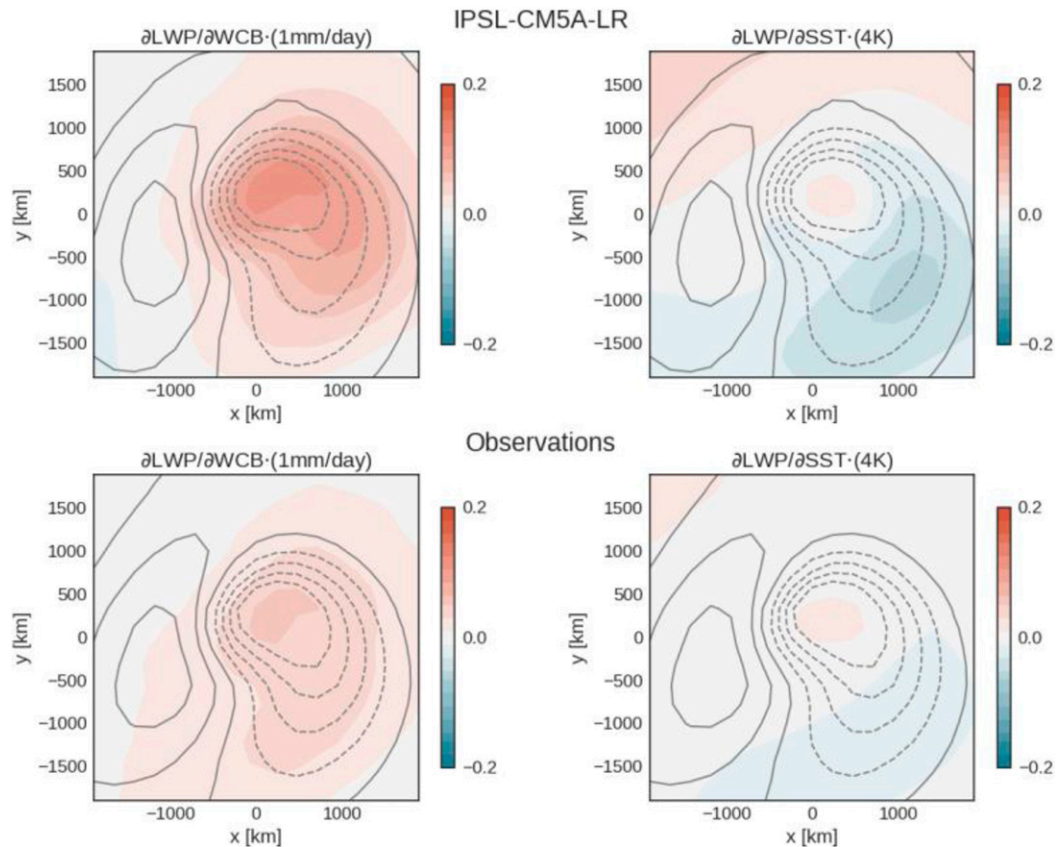


FIG. 7. Regression coefficients relating cyclone SST and WCB moisture convergence to LWP within the cyclone for IPSL-CM5A-LR and the observational record. Gray contours show subsidence as in Fig. 6. Equivalent figures for the remaining GCMs are shown in Fig. S6. Regression coefficients are scaled by the approximate change in WCB moisture convergence (1 mm day^{-1}) and SST (4 K) between AMIP and AMIP + 4 K simulations to facilitate comparison to Fig. 6.

localization of this response to warming and relatively strong sensitivity of LWP to WCB moisture flux in several of the GCMs examined in this study is consistent with the analysis presented in Kelleher and Grise (2019), which showed too strong a sensitivity of shortwave cloud radiative effect to vertical velocity. Increased SST covaries with increased LWP on the poleward side of the cyclone and decreased LWP on the equatorward side. This may be consistent with ice to liquid transitions (Tan et al. 2016) and buoyancy-driven thinning of boundary layer cloud (Bretherton and Blossey 2014), respectively. The spatial pattern of the covariances between LWP, SST, and WCB moisture convergence are found to be qualitatively similar between the observations and GCMs (Fig. S6) and sum to be consistent with the change in LWP between AMIP and AMIP + 4 K (Fig. S5). Observations do not infer a substantial increase in LWP in response to increased SST on the poleward flank of cyclones compared to GCMs (Fig. S6). If this behavior in GCMs is tied to mixed-phase clouds, then this is also consistent with observations of a weak response in cloud-top phase to warming in this region of cyclones (McCoy et al. 2019). Targetted analysis of

frontal behavior using estimates of phase and precipitation from active remote sensing could provide an avenue toward constraining the effects of precipitation efficiency and phase (Naud et al. 2012).

b. Outside of cyclones

1) CLOUD CONTROLLING FACTOR PREDICTION OF CHANGES IN LIQUID WATER PATH

Following the analysis of cyclone properties shown in section 3a, we train the multiple linear regression model shown in Eq. (1) on GCM output and observations outside of cyclones. The coefficients relating meteorological predictors to LWP in 2-K -wide bins of SST are shown in Fig. 8. The coefficients relating SST and $\omega_{500\text{hPa}}$ to LWP (Figs. 8a,c) are qualitatively consistent with the regression model trained inside of cyclones, and with previous literature (Klein et al. 2017). The $c_{\text{FW07}} \times \text{WVP} \times U_{10\text{m}}$ is found to positively covary with LWP (Fig. 8d)—consistent with Fig. 2d. Broadly, this term acts as a diagnostic of water vapor advection and precipitation (Fig. S2) and a positive correlation with LWP is consistent with the mechanism shown in Fig. 3.

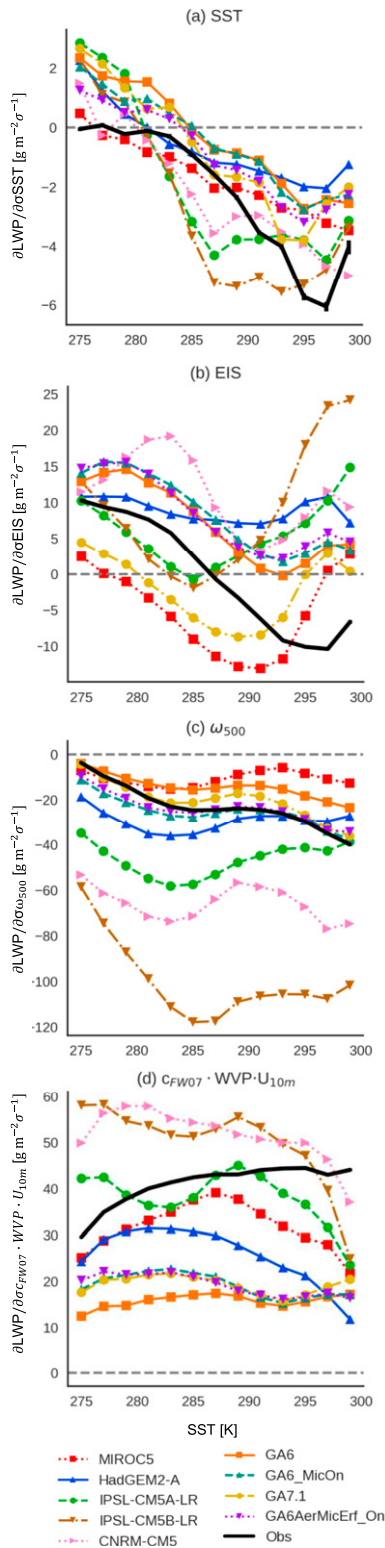


FIG. 8. As in Fig. 2, but for out-of-cyclone clouds. The same figure without normalizing the coefficients by standard deviation in CCF for each bin of SST is shown in Fig. S7.

The relationship between boundary layer stability (EIS) and LWP is not consistent in sign between GCMs (Fig. 8b). The sign of the relationship between EIS and LWP in a given model is consistent with the behavior in cyclone clouds (Fig. 2b). The relationship diagnosed from observations transitions from positive at low SST to negative at high SST. A positive relationship between EIS and LWP is consistent with intuition based on previous analysis of subtropical cloud fraction (D. T. McCoy et al. 2017; Qu et al. 2015; Wood and Bretherton 2006) and the optical depth of extratropical stratus clouds (Terai et al. 2016; Terai et al. 2019). The SST dependence of $\partial\text{LWP}/\partial\text{EIS}$ is also consistent with the sensitivity of extratropical low cloud cover to EIS when temperature advection is held constant (Zelinka et al. 2018). However, direct comparison between these studies and the present study is not possible. The aforementioned analyses focused on different cloud regimes, consider fewer CCFs, and examined in-cloud LWP, optical depth, and cloud fraction instead of area-mean LWP (i.e., cloud liquid water path averaged over cloudy and clear; see section 2a). One possibility is that EIS increasing affects the cloud field by either decreasing LWP inside of cumulus clouds, or results in a shift in cloud regime. For example, it is possible that increased stability results in a shift toward from open cellular convection and cumuliform cloud toward closed cells and stratus clouds, which may have an overall lower LWP (I. L. McCoy et al. 2017). Due to difficulties in retrieving cloud optical depth in open cellular convection or cumulus this sort of transition would not necessarily appear in an analysis of the cloud optical depth and in-cloud LWP that can be observed in overcast stratus clouds (Terai et al. 2016, 2019). Decreased LWP in response to increased EIS is consistent with a positive correlation between EIS and shortwave cloud radiative effect on the equatorward side of the midlatitudes found in Kelleher and Grise (2019), which is also consistent with the in-cyclone behavior shown in Fig. S6. The increase in the strength of the positive relationship observed between LWP and EIS out of cyclones over lower SST (Fig. S7), and in cyclones on their poleward flank (Fig. S6) is also consistent with the negative correlation between EIS and shortwave cloud radiative effect found by Kelleher and Grise (2019) in the poleward portions of the midlatitudes.

Following the same technique as in section 3a(1), we predict the change in LWP based on the regression models trained on present-day variability to predict the difference in LWP between the AMIP and AMIP + 4 K simulations. The only difference in methodology from section 3a(1) is that CCFs from the AMIP and AMIP + 4 K simulations are averaged to monthly means at $1^\circ \times 1^\circ$ before multiplying by the sensitivity of LWP to each CCF. This finer averaging grid is due to the much larger data volume of $1^\circ \times 1^\circ$ data outside of cyclones as opposed to 2000-km-radius cyclone means. The change in LWP outside of cyclones between AMIP and AMIP + 4 K predicted by the regression model agrees with the actual GCM response to increased SST (Fig. 9). In keeping with cyclones, almost all the model response in LWP outside of cyclones is due to increases in $c_{\text{FW07}} \times \text{WVP} \times U_{10\text{m}}$ and SST. Increased $c_{\text{FW07}} \times \text{WVP} \times U_{10\text{m}}$ predicts increased LWP at all latitudes, while increased SST predicts decreased LWP toward the

Change in LWP between AMIP and AMIP+4K as predicted by regression model out-of-cyclones

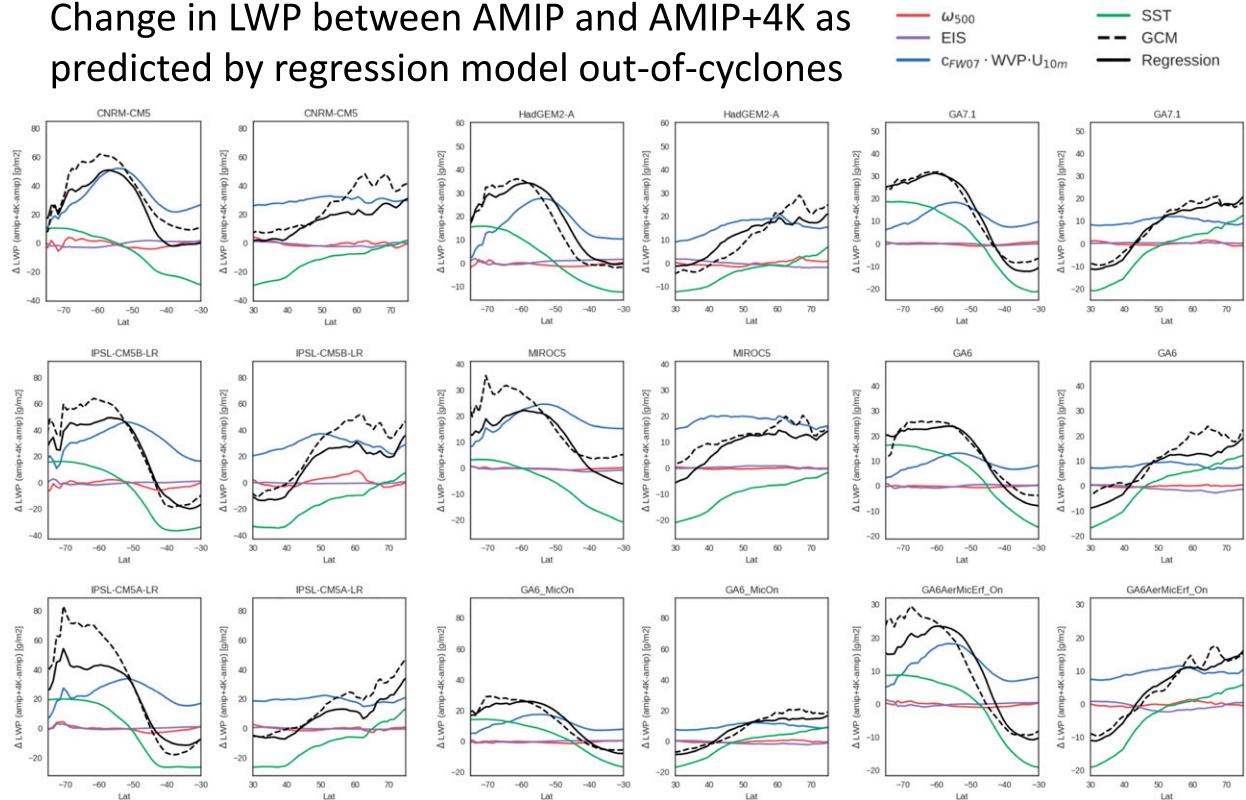


FIG. 9. As in Fig. 4, but showing results for out-of-cyclone clouds.

equator with slight increases in LWP toward the poles in some models.

Figure 10 shows the change in LWP between AMIP and AMIP + 4 K simulations averaged over the 35°–75°S and 35°–75°N oceanic latitude bands and weighted by the RFO of out-of-cyclone states. Observational constraints are created by combining the regression model trained in the observational record with the modeled change in CCFs for all the GCMs. The change in out-of-cyclone LWP is around a third of the response of in-cyclone LWP (Fig. 5) and is between 0.6 and 2.1 $\text{g m}^{-2} \text{K}^{-1}$ (NH) and 1.8 and 3.7 $\text{g m}^{-2} \text{K}^{-1}$ (SH) (Fig. 10). As in section 3a(1), the range in the observational constraint combines uncertainty in the change in CCFs between AMIP and AMIP + 4 K (red and blue shading in Fig. 10) and uncertainty in the prediction of the true change in LWP in models by the multiple linear regression model (gray shading around the best fit line in Fig. 10).

2) EXPLORING PHYSICAL MECHANISMS IN HADGEM3 MODEL VARIANTS

As discussed in section 3a, one hypothesized explanation of extratropical changes in LWP with warming has been deglaciation in cold clouds. We find that moisture advection and SST changes appear to dominate the extratropical changes in LWP outside of cyclones. As in section 3a(b), we turn to examining the HadGEM3-GA7.1 development models where different packages are switched on one at a time. As discussed in section 3a(2), the progression of changes from GA6, to GA6_

MicOn, to GA6AerMicErf_On increases the amount of supercooled liquid water in the extratropics (Furtado and Field 2017). It seems likely that enhancing supercooled liquid should suppress deglaciation with warming because there will be less glaciated cloud to affect. $\partial\text{LWP}/\partial(c_{\text{FW07}} \times \text{WVP} \times U_{10\text{m}})$ and $\partial\text{LWP}/\partial\text{SST}$ only change modestly as the mixed-phase cloud scheme is altered (Figs. S7a,d). The lack of sensitivity in either term to changes in mixed-phase parameterization suggests that feedbacks due to deglaciation in mixed-phase clouds do not play a dominant role in changes in LWP outside of cyclones, but as noted in section 3a(2), similar sensitivity studies in other GCMs are needed.

c. Change in extratropical albedo

1) OBSERVED RELATIONSHIP BETWEEN AREA-MEAN LWP AND ALBEDO

Sections 3a and 3b examined the change in area-mean LWP between AMIP and AMIP + 4 K simulations inside and out of extratropical cyclones. Analyzing LWP has several advantages. First, it adds diversity to the literature on constraining cloud feedbacks. Low-frequency microwave remote sensing algorithms are largely insensitive to ice overlaying liquid cloud and are equally influenced by the entire columnar profile of liquid, with little sensitivity to the altitude at which the liquid cloud is occurring in contrast to spectroradiometer retrievals of liquid clouds made at other frequencies that have been used by

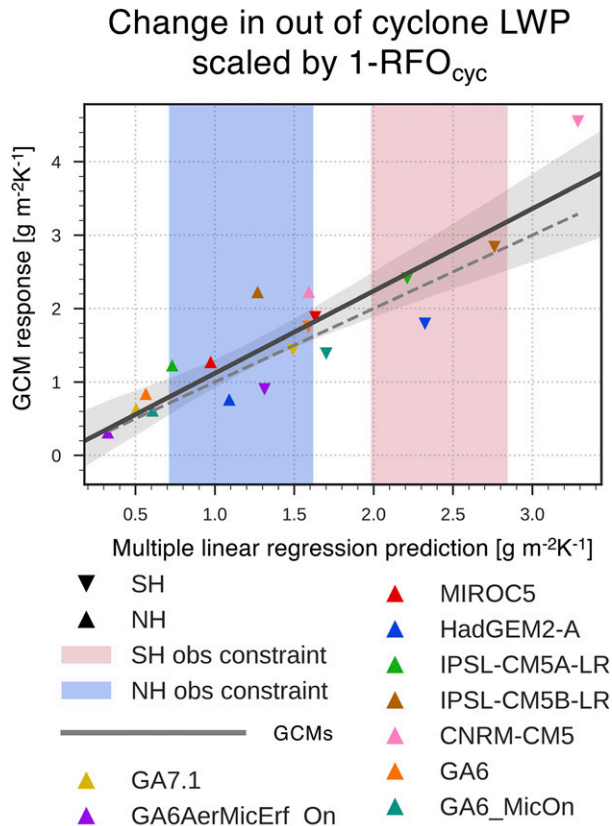


FIG. 10. As in Fig. 5, but for out-of-cyclone clouds. The change in LWP is now weighted by the RFO for out-of-cyclone clouds.

several previous constraint studies (Gordon and Klein 2014; Terai et al. 2019; Tselioudis et al. 1992). This provides a useful contrast to these studies and extends analysis in Ceppi et al. (2016b). Second, we argue that microwave retrievals are somewhat better suited for studying clouds in the mid-high latitudes relative to visible and near-infrared retrievals. Microwave LWP retrievals are insensitive to near-horizon SZA, multiple cloud layers, and broken cloud cover—all of which are frequent in the midlatitude storm tracks (Haynes et al. 2011). Finally, microwave LWP is analogous to the LWP output by GCMs. While useful for the reasons outlined above, microwave LWP cannot be directly linked to changes in top-of-atmosphere SW radiation in the same way as cloud optical depth. This link is critical to making statements about the SW cloud feedback because LWP changes will not always affect shortwave radiation in the same way (if the sun is not overhead, for example).

We now present an estimate of the extent to which changes in LWP will affect outgoing SW in the extratropics using the empirical relationship between albedo and LWP in the present climate to predict how changes in LWP in the future will translate to changes in SW.

Albedo data are obtained from the CERES SYN1deg, edition 4 (Doelling et al. 2016, 2013), dataset. The regression of albedo on LWP is calculated to quantify the sensitivity of

albedo to variations in LWP. As noted in section 2a, all data collected where $SZA > 45^\circ$ are disregarded. This reduces, but does not entirely remove, albedo dependence on SZA (see Fig. 2 of McCoy et al. 2018b). To further moderate the dependence of albedo on SZA we examine the regression of albedo on LWP independently in each month of the year and in ten bins of latitude between $70^\circ S$ and $70^\circ N$. As in section 3a, daily mean cyclone-mean quantities are used to train the regression for data identified as being within 2000 km of a cyclone center. As in section 3b, outside of cyclones $1^\circ \times 1^\circ$ daily mean data are used to train the regression. All analyses discussed in this section were performed as a function of latitude and month of the year, as well as for inside- and outside-cyclone regions as defined above.

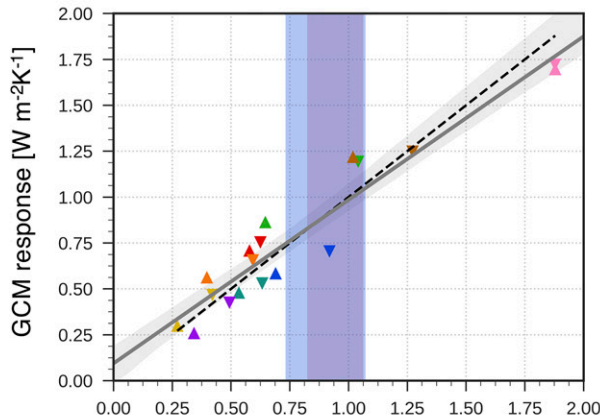
The relationship between albedo α and LWP is found to be nearly linear for regions within and outside of cyclone boundaries. Assuming that in-cloud LWP is approximately constant, this is consistent with the microwave LWP being proportional to the product of cloud fraction and in-cloud LWP, and the linear dependence of albedo on cloud fraction (Bender et al. 2016). Regression coefficients ($da/dLWP$) are shown in Fig. S8; $da/dLWP$ tends to be larger in cyclones. Also, $da/dLWP$ for cyclones is near zero or negative only at low sun angles around local winter (Fig. S8a). In local summer when insolation is strongest $da/dLWP$ tends to be larger inside and outside of cyclones. In this study we use the medians of $da/dLWP$ inside and outside cyclones to relate changes in LWP to changes in albedo.

Outside of cyclones, the relationship between boundary layer liquid cloud cover and albedo is relatively straightforward since these regions do not have a complex vertical cloud structure, whereas in cyclones, frontal structures lead to more complexity in cloud shields. This complicates the relationship between top-of-atmosphere radiation and LWP in cyclones. One potential concern with this analysis is that albedo fluctuations in cyclones are controlled by changes in cloud shields or other ice clouds and a regression between LWP and albedo will not be a useful way to understand future changes in albedo. Below we present analysis to show that the relationship between meteorology and albedo is moderated by LWP.

As discussed in section 3a, most of the climate response in extratropical cyclone LWP originates from changes in the WCB moisture flux. Thus, a simpler question might be whether albedo changes with WCB moisture flux. To answer this question, we regress cyclone-mean albedo on WCB moisture flux ($da/dWCB$). This yields a relationship between the synoptic state and albedo. Does this relationship between albedo and meteorology break down if we recalculate it using the sensitivity of LWP to WCB moisture flux, and the sensitivity of albedo to LWP? The regression of cyclone-mean LWP on WCB moisture flux ($dLWP/dWCB$) is multiplied by $da/dLWP$. This is done as a function of latitude and month, as in Fig. S8a. This analysis shows that WCB moisture flux affects albedo via perturbations in LWP (Fig. S9). The agreement between these calculations is good, supporting the use of the regression of albedo on LWP in cyclones to calculate changes in albedo due to changes in LWP between AMIP and AMIP + 4K.

Change in upwelling SW scaled by RFO

(a) Cyclone



(b) Out of cyclone

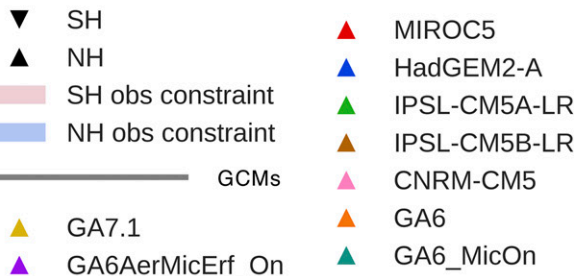
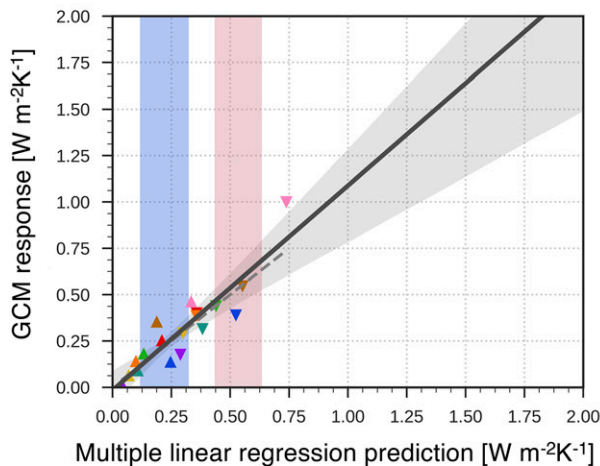


FIG. 11. As in Fig. 5, but showing the projected change in shortwave consistent with the change in LWP between AMIP and AMIP + 4 K for (a) cyclones and (b) out of cyclones. The change in shortwave is shown weighted by the relative frequency of occurrence of cyclones in (a) and out of cyclones in (b). The change in shortwave is calculated based on the empirical relationship between albedo and LWP in observations (Fig. S8).

2) PROJECTION OF UPWELLING SHORTWAVE FROM CHANGES IN LWP

Change in SW in response to change in LWP is calculated by scaling the change in LWP between AMIP and AMIP + 4 K simulations calculated in sections 3a and 3b by the median of $da/dLWP$ across months and latitude bins (Fig. S8). LWP changes inside and outside of cyclones are scaled by the median $da/dLWP$ observed inside and outside of cyclones, respectively. The predicted change in albedo is then scaled by the downwelling SW resolved in latitude and month to calculate the change in reflected SW. This is shown in Fig. 11 averaged over the 35°–75°S and 35°–75°N latitude bands. As in Figs. 5 and 10, changes in SW are shown weighted by the RFO of cyclone and out-of-cyclone states. The change in SW is dominated by changes in cyclones. The best estimate of the change in SW in cyclones in the NH is 0.7–1.2 and 0.8–1.1 $W m^{-2} K^{-1}$ in the SH. Outside of cyclones it is 0.1–0.4 $W m^{-2} K^{-1}$ in the NH and 0.4–0.8 $W m^{-2} K^{-1}$ in the SH. Combining inside- and outside-cyclone states results in a best estimate of an increase in outgoing SW in response to uniform surface warming. The minimum change in SW from inside and outside of cyclones is 0.8 $W m^{-2} K^{-1}$ over NH oceans between 35°N and 75°N and 1.2 $W m^{-2} K^{-1}$ over SH oceans between 35°S and 75°S. The maximum change in SW from inside and outside of cyclones is 1.6 $W m^{-2} K^{-1}$ in the NH and 1.9 $W m^{-2} K^{-1}$ in the SH. These calculations are performed analogously to Figs. 5 and 10 but summing Figs. 11a and 11b to get a total change in SW.

4. Summary

In this work we present a constraint on extratropical cloud feedback that is designed within the framework of extratropical weather regimes. We extend previous work contrasting observed and modeled extratropical regimes (Bodas-Salcedo et al. 2014) to examine what meteorological predictors play a key role in the climate response of clouds in the extratropics. This work also complements the daily time scale analysis of relationships between CCFs and SW cloud radiative forcing by Kelleher and Grise (2019). The central dataset used in this study is microwave area-mean (averaged across regions with cloud and without cloud) LWP as observed by MAC-LWP. We used multiple linear regression models trained in the present-day (AMIP) simulations to predict GCM responses to increased SST (AMIP + 4 K). This was combined with multiple linear regression models trained on observations in the present day to offer constraints on GCM behavior. It is found that almost all the change in LWP in the extratropics can be traced to increasing SST and increased moisture (Fig. 4, Fig. S3, and Fig. 9). The change in LWP was calculated from the observational constraints within each regime by adding their minimums and maximums, respectively. This yields an increase in LWP inside and outside of cyclones of 4.5–7.6 $g m^{-2} K^{-1}$ in the SH (35°–75°S) and 3.2–6.2 $g m^{-2} K^{-1}$ in the NH (35°–75°N). This agrees with the response of LWP to uniform warming presented in Ceppi et al. (2016b) of 0–8 $g m^{-2} K^{-1}$ for the 45°–60°S region. The relative strength of observed trends in LWP over oceans between 44.5° and 59.5°S compared to CMIP5 models diagnosed by Manaster et al. (2017) qualitatively agrees with our results in finding that observations predicted an increase in

LWP on the upper end of CMIP5 models, but a direct comparison is difficult due to a different selection of CMIP5 models.

Using an empirical relationship between observations of albedo and LWP we estimate that over oceans between 35° and 75°S increased LWP increases reflected SW by 1.2–1.9 W m⁻² K⁻¹, which agrees with the constraint calculated using CTP optical depth histograms in Ceppi et al. (2016b) of 0–2 W m⁻² K⁻¹. This result appears to conflict with the decreasing cloud optical depth between 40° and 70°S predicted by Terai et al. (2016). However, as pointed out in Terai et al. (2016) this is because their analysis focused on changes in optical depth for low, stratiform clouds, in contrast to the present study and Ceppi et al. (2016b), which examine cloud variability at all cloud-top pressures and considered changes in cloud extent. These differing results imply that the cloud feedback within the low, stratiform regime in the extratropics acts to oppose changes in other regimes. The synthesis of these results agrees with the analysis presented in Tan et al. (2019), which showed decreasing optical depth in warm, liquid clouds and increasing cloud optical depth in cold clouds. This is consistent with the increased LWP in regions of ascent driven by moisture convergence diagnosed in this study (Fig. 6, Fig. S5, Fig. S6, and Fig. 7). Overall, this study and past constraint studies agree in excluding models with strongly negative SW cloud feedbacks such as CNRM-CM5, or IPSL-CM5B-LR, while showing that models with weaker SW cloud feedbacks such as IPSL-CM5A-LR, and HadGEM2-A are consistent with observations. This is inferred based on the results shown in Fig. 11 as well as comparing to the full SW cloud feedback decompositions for these and other models (shown in Fig. S6 of Zelinka et al. 2020). Further analysis to unify the analysis of low, liquid-topped clouds in Terai et al. (2016), and the analysis presented here and in Ceppi et al. (2016b) is needed.

The majority of the change in extratropical LWP was found to be due to increased cyclone LWP driven by increased WCB moisture flux, in turn driven by increased WVP following Clausius–Clapeyron. The relationship between cyclone LWP and WCB moisture flux can be characterized observationally. This will allow modeling centers to evaluate the sensitivity of LWP to meteorological state in their models, in turn constraining their extratropical SW cloud feedback. One intriguing possibility is that some of the diagnosed shift toward higher climate sensitivity through decreased extratropical cloud feedback between CMIP5 and CMIP6 (Zelinka et al. 2020) may be due to increased efficiency in converting converging moisture to precipitation. The comparison between a small selection of GCMs from CMIP5 and CMIP6 shown in McCoy et al. (2019) suggests that this might be the case with generally lower sensitivity of LWP to WCB moisture flux diagnosed in CMIP6 models. This is also consistent with too strong a sensitivity of shortwave cloud radiative effect to vertical velocity in CMIP5 models and, by extension, fronts that brighten too much in response to changes in dynamics (Kelleher and Grise 2019). However, the small number of models with appropriate daily resolution data needed to perform the analysis presented here is too small to definitively conclude this about the entirety of CMIP5 and CMIP6.

We believe that the analysis presented in this study supports a robustly negative SW cloud feedback in the extratropics originating from enhanced moisture flux into cyclones driven by Clausius–Clapeyron. This feature is a function of the efficacy with which cyclones can convert converging moisture into precipitation, and thus we believe that refinement of precipitation processes in cyclones is a promising avenue of investigation to constrain extratropical cloud feedbacks.

Acknowledgments. We thank the efforts of three anonymous reviewers and editor Isaac Held in improving this work. DTM and PRF acknowledge support from the PRIMAVERA project, funded by the European Union's Horizon 2020 Programme, Grant Agreement 641727. GSE acknowledges support from the NASA Data for Operations and Assessment (Grant NNX17AF46G) and NASA Science of Terra, Aqua, and Suomi NPP (TASNPP; Grant 80NSSC18K1030) programs. The work of M.D.Z. was performed under the auspices of the U.S. Department of Energy (DOE) by Lawrence Livermore National Laboratory under Contract DE-AC52-07 NA27344 and was supported by the Regional and Global Model Analysis Program of the Office of Science at the DOE. ABS work was supported by the Met Office Hadley Centre Climate Programme funded by BEIS and Defra.

REFERENCES

- Baker, A. J., and Coauthors, 2019: Enhanced climate change response of wintertime North Atlantic circulation, cyclonic activity, and precipitation in a 25-km-resolution global atmospheric model. *J. Climate*, **32**, 7763–7781, <https://doi.org/10.1175/JCLI-D-19-0054.1>.
- Bender, F. A. M., A. Engström, and J. Karlsson, 2016: Factors controlling cloud albedo in marine subtropical stratocumulus regions in climate models and satellite observations. *J. Climate*, **29**, 3559–3587, <https://doi.org/10.1175/JCLI-D-15-0095.1>.
- Betts, A. K., and Harshvardhan, 1987: Thermodynamic constraint on the cloud liquid water feedback in climate models. *J. Geophys. Res.*, **92**, 8483–8485, <https://doi.org/10.1029/JD092iD07p08483>.
- Blossey, P. N., and Coauthors, 2013: Marine low cloud sensitivity to an idealized climate change: The CGILS LES intercomparison. *J. Adv. Model. Earth Syst.*, **5**, 234–258, <https://doi.org/10.1002/jame.20025>.
- Bodas-Salcedo, A., 2018: Cloud condensate and radiative feedbacks at midlatitudes in an aquaplanet. *Geophys. Res. Lett.*, **45**, 3635–3643, <https://doi.org/10.1002/2018GL077217>.
- , and Coauthors, 2014: Origins of the solar radiation biases over the Southern Ocean in CFMIP2 models. *J. Climate*, **27**, 41–56, <https://doi.org/10.1175/JCLI-D-13-00169.1>.
- , J. P. Mulcahy, T. Andrews, K. D. Williams, M. A. Ringer, P. R. Field, and G. S. Elsaesser, 2019: Strong dependence of atmospheric feedbacks on mixed-phase microphysics and aerosol-cloud interactions in HadGEM3. *J. Adv. Model. Earth Syst.*, **11**, 1735–1758, <https://doi.org/10.1029/2019MS001688>.
- Bony, S., M. Webb, C. Bretherton, S. Klein, P. Siebesma, G. Tselioudis, and M. Zhang, 2011: CFMIP: Towards a better evaluation and understanding of clouds and cloud feedbacks in CMIP5 models. *CLIVAR Exchanges*, No. 56, International CLIVAR Project Office, Southampton, United Kingdom, 20–22.
- Bretherton, C. S., 2015: Insights into low-latitude cloud feedbacks from high-resolution models. *Philos. Trans. Roy. Soc. London*, **A373**, 20140415, <https://doi.org/10.1098/RSTA.2014.0415>.

- , and P. N. Blossey, 2014: Low cloud reduction in a greenhouse-warmed climate: Results from Lagrangian LES of a subtropical marine cloudiness transition. *J. Adv. Model. Earth Syst.*, **6**, 91–114, <https://doi.org/10.1002/2013MS000250>.
- , M. E. Peters, and L. E. Back, 2004: Relationships between water vapor path and precipitation over the tropical oceans. *J. Climate*, **17**, 1517–1528, [https://doi.org/10.1175/1520-0442\(2004\)017<1517:RBWVPA>2.0.CO;2](https://doi.org/10.1175/1520-0442(2004)017<1517:RBWVPA>2.0.CO;2).
- , P. N. Blossey, and C. R. Jones, 2013: Mechanisms of marine low cloud sensitivity to idealized climate perturbations: A single-LES exploration extending the CGILS cases. *J. Adv. Model. Earth Syst.*, **5**, 316–337, <https://doi.org/10.1002/jame.20019>.
- Caldwell, P. M., M. D. Zelinka, K. E. Taylor, and K. Marvel, 2016: Quantifying the sources of intermodel spread in equilibrium climate sensitivity. *J. Climate*, **29**, 513–524, <https://doi.org/10.1175/JCLI-D-15-0352.1>.
- Catto, J. L., C. Jakob, G. Berry, and N. Nicholls, 2012: Relating global precipitation to atmospheric fronts. *Geophys. Res. Lett.*, **39**, L10805, <https://doi.org/10.1029/2012GL051736>.
- Ceppi, P., D. L. Hartmann, and M. J. Webb, 2016a: Mechanisms of the negative shortwave cloud feedback in middle to high latitudes. *J. Climate*, **29**, 139–157, <https://doi.org/10.1175/JCLI-D-15-0327.1>.
- , D. T. McCoy, and D. L. Hartmann, 2016b: Observational evidence for a negative shortwave cloud feedback in middle to high latitudes. *Geophys. Res. Lett.*, **43**, 1331–1339, <https://doi.org/10.1002/2015GL067499>.
- , F. Briant, M. D. Zelinka, and D. L. Hartmann, 2017: Cloud feedback mechanisms and their representation in global climate models. *Wiley Interdiscip. Rev.: Climate Change*, **8**, e465, <https://doi.org/10.1002/WCC.465>.
- Clement, A. C., R. Burgman, and J. R. Norris, 2009: Observational and model evidence for positive low-level cloud feedback. *Science*, **325**, 460–464, <https://doi.org/10.1126/science.1171255>.
- Collins, W. J., and Coauthors, 2011: Development and evaluation of an Earth-system model—HadGEM2. *Geosci. Model Dev.*, **4**, 1051–1075, <https://doi.org/10.5194/gmd-4-1051-2011>.
- Davini, P., S. Corti, F. D’Andrea, G. Rivière, and J. von Hardenberg, 2017: Improved winter European atmospheric blocking frequencies in high-resolution global climate simulations. *J. Adv. Model. Earth Syst.*, **9**, 2615–2634, <https://doi.org/10.1002/2017MS001082>.
- Doelling, D. R., and Coauthors, 2013: Geostationary enhanced temporal interpolation for CERES flux products. *J. Atmos. Oceanic Technol.*, **30**, 1072–1090, <https://doi.org/10.1175/JTECH-D-12-00136.1>.
- , C. O. Haney, B. R. Scarino, A. Gopalan, and R. Bhatt, 2016: Improvements to the geostationary visible imager ray-matching calibration algorithm for CERES edition 4. *J. Atmos. Oceanic Technol.*, **33**, 2679–2698, <https://doi.org/10.1175/JTECH-D-16-0113.1>.
- Dufresne, J.-L., and Coauthors, 2013: Climate change projections using the IPSL-CM5 Earth System Model: From CMIP3 to CMIP5. *Climate Dyn.*, **40**, 2123–2165, <https://doi.org/10.1007/s00382-012-1636-1>.
- Elsaesser, G. S., C. W. O’Dell, M. D. Lebsock, R. Bennartz, T. J. Greenwald, and F. J. Wentz, 2017: The Multi-Sensor Advanced Climatology of Liquid Water Path (MAC-LWP). *J. Climate*, **30**, 10 193–10 210, <https://doi.org/10.1175/JCLI-D-16-0902.1>.
- Eyring, V., S. Bony, G. A. Meehl, C. A. Senior, B. Stevens, R. J. Stouffer, and K. E. Taylor, 2016: Overview of the Coupled Model Intercomparison Project Phase 6 (CMIP6) experimental design and organization. *Geosci. Model Dev.*, **9**, 1937–1958, <https://doi.org/10.5194/gmd-9-1937-2016>.
- Field, P. R., and R. Wood, 2007: Precipitation and cloud structure in midlatitude cyclones. *J. Climate*, **20**, 233–254, <https://doi.org/10.1175/JCLI3998.1>.
- , and A. J. Heymsfield, 2015: Importance of snow to global precipitation. *Geophys. Res. Lett.*, **42**, 9512–9520, <https://doi.org/10.1002/2015GL065497>.
- , A. Gettelman, R. B. Neale, R. Wood, P. J. Rasch, and H. Morrison, 2008: Midlatitude cyclone compositing to constrain climate model behavior using satellite observations. *J. Climate*, **21**, 5887–5903, <https://doi.org/10.1175/2008JCLI2235.1>.
- , A. Bodas-Salcedo, and M. E. Brooks, 2011: Using model analysis and satellite data to assess cloud and precipitation in midlatitude cyclones. *Quart. J. Roy. Meteor. Soc.*, **137**, 1501–1515, <https://doi.org/10.1002/qj.858>.
- Furtado, K., and P. Field, 2017: The role of ice microphysics parametrizations in determining the prevalence of supercooled liquid water in high-resolution simulations of a Southern Ocean midlatitude cyclone. *J. Atmos. Sci.*, **74**, 2001–2021, <https://doi.org/10.1175/JAS-D-16-0165.1>.
- , —, I. A. Boutle, C. J. Morcrette, and J. M. Wilkinson, 2016: A physically based subgrid parameterization for the production and maintenance of mixed-phase clouds in a general circulation model. *J. Atmos. Sci.*, **73**, 279–291, <https://doi.org/10.1175/JAS-D-15-0021.1>.
- Gilmore, J. B., 2015: Understanding the influence of measurement uncertainty on the atmospheric transition in rainfall and column water vapor. *J. Atmos. Sci.*, **72**, 2041–2054, <https://doi.org/10.1175/JAS-D-14-0211.1>.
- Gonzalez, P. L. M., D. J. Brayshaw, and G. Zappa, 2019: The contribution of North Atlantic atmospheric circulation shifts to future wind speed projections for wind power over Europe. *Climate Dyn.*, **53**, 4095–4113, <https://doi.org/10.1007/s00382-019-04776-3>.
- Gordon, N. D., and S. A. Klein, 2014: Low-cloud optical depth feedback in climate models. *J. Geophys. Res. Atmos.*, **119**, 6052–6065, <https://doi.org/10.1002/2013JD021052>.
- Harrold, T. W., 1973: Mechanisms influencing the distribution of precipitation within baroclinic disturbances. *Quart. J. Roy. Meteor. Soc.*, **99**, 232–251, <https://doi.org/10.1002/qj.49709942003>.
- Hartmann, D. L., and D. A. Short, 1980: On the use of Earth radiation budget statistics for studies of clouds and climate. *J. Atmos. Sci.*, **37**, 1233–1250, [https://doi.org/10.1175/1520-0469\(1980\)037<1233:OTUOER>2.0.CO;2](https://doi.org/10.1175/1520-0469(1980)037<1233:OTUOER>2.0.CO;2).
- Haynes, J. M., C. Jakob, W. B. Rossow, G. Tselioudis, and J. Brown, 2011: Major characteristics of Southern Ocean cloud regimes and their effects on the energy budget. *J. Climate*, **24**, 5061–5080, <https://doi.org/10.1175/2011JCLI4052.1>.
- Hirata, H., R. Kawamura, M. Kato, and T. Shinoda, 2016: Response of rapidly developing extratropical cyclones to sea surface temperature variations over the western Kuroshio–Oyashio confluence region. *J. Geophys. Res. Atmos.*, **121**, 3843–3858, <https://doi.org/10.1002/2015JD024391>.
- Hourdin, F., and Coauthors, 2013: LMDZ5B: The atmospheric component of the IPSL climate model with revisited parameterizations for clouds and convection. *Climate Dyn.*, **40**, 2193–2222, <https://doi.org/10.1007/s00382-012-1343-y>.
- Jiang, J. H., and Coauthors, 2012: Evaluation of cloud and water vapor simulations in CMIP5 climate models using NASA “A-Train” satellite observations. *J. Geophys. Res.*, **117**, D14105, <https://doi.org/10.1029/2011JD017237>.
- Jiaxiang, G., and Coauthors, 2020: Influence of model resolution on bomb cyclones revealed by HighResMIP-PRIMAVERA simulations. *Environ. Res. Lett.*, **15**, 084001, <https://doi.org/10.1088/1748-9326/ab88fa>.

- Kay, J. E., C. Wall, V. Yettella, B. Medeiros, C. Hannay, P. Caldwell, and C. Bitz, 2016: Global climate impacts of fixing the Southern Ocean shortwave radiation bias in the Community Earth System Model (CESM). *J. Climate*, **29**, 4617–4636, <https://doi.org/10.1175/JCLI-D-15-0358.1>.
- Kelleher, M. K., and K. M. Grise, 2019: Examining Southern Ocean cloud controlling factors on daily time scales and their connections to midlatitude weather systems. *J. Climate*, **32**, 5145–5160, <https://doi.org/10.1175/JCLI-D-18-0840.1>.
- Klein, S. A., D. L. Hartmann, and J. R. Norris, 1995: On the relationships among low-cloud structure, sea surface temperature, and atmospheric circulation in the summertime northeast Pacific. *J. Climate*, **8**, 1140–1155, [https://doi.org/10.1175/1520-0442\(1995\)008<1140:OTRALC>2.0.CO;2](https://doi.org/10.1175/1520-0442(1995)008<1140:OTRALC>2.0.CO;2).
- , A. Hall, J. R. Norris, and R. Pincus, 2017: Low-cloud feedbacks from cloud-controlling factors: A review. *Surv. Geophys.*, **38**, 1307–1329, <https://doi.org/10.1007/s10712-017-9433-3>.
- Loeb, N. G., B. A. Wielicki, D. R. Doelling, G. L. Smith, D. F. Keyes, S. Kato, N. Manalo-Smith, and T. Wong, 2009: Toward optimal closure of the Earth's top-of-atmosphere radiation budget. *J. Climate*, **22**, 748–766, <https://doi.org/10.1175/2008JCLI2637.1>.
- Manaster, A., C. W. O'Dell, and G. Elsaesser, 2017: Evaluation of cloud liquid water path trends using a multidecadal record of passive microwave observations. *J. Climate*, **30**, 5871–5884, <https://doi.org/10.1175/JCLI-D-16-0399.1>.
- Martin, G. M., and Coauthors, 2011: The HadGEM2 family of Met Office Unified Model climate configurations. *Geosci. Model Dev.*, **4**, 723–757, <https://doi.org/10.5194/gmd-4-723-2011>.
- McCoy, D. T., D. L. Hartmann, M. D. Zelinka, P. Ceppi, and D. P. Grosvenor, 2015: Mixed-phase cloud physics and Southern Ocean cloud feedback in climate models. *J. Geophys. Res. Atmos.*, **120**, 9539–9554, <https://doi.org/10.1002/2015JD023603>.
- , R. Eastman, D. L. Hartmann, and R. Wood, 2017: The change in low cloud cover in a warmed climate inferred from AIRS, MODIS, and ERA-Interim. *J. Climate*, **30**, 3609–3620, <https://doi.org/10.1175/JCLI-D-15-0734.1>.
- , D. L. Hartmann, and M. D. Zelinka, 2018a: Mixed-phase cloud feedbacks. *Mixed-Phase Clouds*, C. Andronache, Ed., Elsevier, 215–236.
- , and Coauthors, 2018b: Aerosol midlatitude cyclone indirect effects in observations and high-resolution simulations. *Atmos. Chem. Phys.*, **18**, 5821–5846, <https://doi.org/10.5194/acp-18-5821-2018>.
- , and Coauthors, 2019: Cloud feedbacks in extratropical cyclones: Insight from long-term satellite data and high-resolution global simulations. *Atmos. Chem. Phys.*, **19**, 1147–1172, <https://doi.org/10.5194/acp-19-1147-2019>.
- , P. Field, H. Gordon, G. S. Elsaesser, and D. P. Grosvenor, 2020: Untangling causality in midlatitude aerosol–cloud adjustments. *Atmos. Chem. Phys.*, **20**, 4085–4103, <https://doi.org/10.5194/acp-20-4085-2020>.
- McCoy, I. L., R. Wood, and J. K. Fletcher, 2017: Identifying meteorological controls on open and closed mesoscale cellular convection associated with marine cold air outbreaks. *J. Geophys. Res. Atmos.*, **122**, 11 678–11 702, <https://doi.org/10.1002/2017JD027031>.
- Mitchell, J. F. B., C. A. Senior, and W. J. Ingram, 1989: CO₂ and climate: A missing feedback. *Nature*, **341**, 132–134, <https://doi.org/10.1038/341132a0>.
- Molod, A., L. Takacs, M. Suarez, and J. Bacmeister, 2015: Development of the GEOS-5 atmospheric general circulation model: Evolution from MERRA to MERRA2. *Geosci. Model Dev.*, **8**, 1339–1356, <https://doi.org/10.5194/gmd-8-1339-2015>.
- Mulcahy, J. P., and Coauthors, 2018: Improved aerosol processes and effective radiative forcing in HadGEM3 and UKESM1. *J. Adv. Model. Earth Syst.*, **10**, 2786–2805, <https://doi.org/10.1029/2018MS001464>.
- Myers, T. A., and J. R. Norris, 2013: Observational evidence that enhanced subsidence reduces subtropical marine boundary layer cloudiness. *J. Climate*, **26**, 7507–7524, <https://doi.org/10.1175/JCLI-D-12-00736.1>.
- , and —, 2015: On the relationships between subtropical clouds and meteorology in observations and CMIP3 and CMIP5 models. *J. Climate*, **28**, 2945–2967, <https://doi.org/10.1175/JCLI-D-14-00475.1>.
- , and —, 2016: Reducing the uncertainty in subtropical cloud feedback. *Geophys. Res. Lett.*, **43**, 2144–2148, <https://doi.org/10.1002/2015GL067416>.
- Naud, C. M., D. J. Posselt, and S. C. van den Heever, 2012: Observational analysis of cloud and precipitation in midlatitude cyclones: Northern versus Southern Hemisphere warm fronts. *J. Climate*, **25**, 5135–5151, <https://doi.org/10.1175/JCLI-D-11-00569.1>.
- Norris, J. R., R. J. Allen, A. T. Evan, M. D. Zelinka, C. W. O'Dell, and S. A. Klein, 2016: Evidence for climate change in the satellite cloud record. *Nature*, **536**, 72–75, <https://doi.org/10.1038/nature18273>.
- Pfahl, S., and M. Sprenger, 2016: On the relationship between extratropical cyclone precipitation and intensity. *Geophys. Res. Lett.*, **43**, 1752–1758, <https://doi.org/10.1002/2016GL068018>.
- Qu, X., A. Hall, S. A. Klein, and A. M. DeAngelis, 2015: Positive tropical marine low-cloud cover feedback inferred from cloud-controlling factors. *Geophys. Res. Lett.*, **42**, 7767–7775, <https://doi.org/10.1002/2015GL065627>.
- Rieck, M., L. Nuijens, and B. Stevens, 2012: Marine boundary layer cloud feedbacks in a constant relative humidity atmosphere. *J. Atmos. Sci.*, **69**, 2538–2550, <https://doi.org/10.1175/JAS-D-11-0203.1>.
- Roberts, M. J., and Coauthors, 2020: Impact of model resolution on tropical cyclone simulation using the HighResMIP-PRIMAVERA multimodel ensemble. *J. Climate*, **33**, 2557–2583, <https://doi.org/10.1175/JCLI-D-19-0639.1>.
- Rushley, S., D. Kim, C. Bretherton, and M. S. Ahn, 2018: Reexamining the nonlinear moisture-precipitation relationship over the tropical oceans. *Geophys. Res. Lett.*, **45**, 1133–1140, <https://doi.org/10.1002/2017GL076296>.
- Stevens, B., and J. L. Brenguier, 2009: Cloud controlling factors: Low clouds. *Clouds in the Perturbed Climate System: Their Relationship to Energy Balance, Atmospheric Dynamics, and Precipitation*, MIT Press, 173–196.
- Tan, I., T. Storelvmo, and M. D. Zelinka, 2016: Observational constraints on mixed-phase clouds imply higher climate sensitivity. *Science*, **352**, 224–227, <https://doi.org/10.1126/science.aad5300>.
- , L. Oreopoulos, and N. Cho, 2019: The role of thermodynamic phase shifts in cloud optical depth variations with temperature. *Geophys. Res. Lett.*, **46**, 4502–4511, <https://doi.org/10.1029/2018GL081590>.
- Taylor, K. E., R. J. Stouffer, and G. A. Meehl, 2012: An overview of CMIP5 and the experiment design. *Bull. Amer. Meteor. Soc.*, **93**, 485–498, <https://doi.org/10.1175/BAMS-D-11-00094.1>.
- Terai, C. R., S. A. Klein, and M. D. Zelinka, 2016: Constraining the low-cloud optical depth feedback at middle and high latitudes using satellite observations. *J. Geophys. Res. Atmos.*, **121**, 9696–9716, <https://doi.org/10.1002/2016JD025233>.
- , Y. Zhang, S. A. Klein, M. D. Zelinka, J. C. Chiu, and Q. Min, 2019: Mechanisms behind the extratropical stratiform

- low-cloud optical depth response to temperature in ARM site observations. *J. Geophys. Res. Atmos.*, **124**, 2127–2147, <https://doi.org/10.1029/2018JD029359>.
- Tselioudis, G., W. B. Rossow, and D. Rind, 1992: Global patterns of cloud optical thickness variation with temperature. *J. Climate*, **5**, 1484–1495, [https://doi.org/10.1175/1520-0442\(1992\)005<1484:GPOCOT>2.0.CO;2](https://doi.org/10.1175/1520-0442(1992)005<1484:GPOCOT>2.0.CO;2).
- Tsushima, Y., and Coauthors, 2006: Importance of the mixed-phase cloud distribution in the control climate for assessing the response of clouds to carbon dioxide increase: A multi-model study. *Climate Dyn.*, **27**, 113–126, <https://doi.org/10.1007/s00382-006-0127-7>.
- Voldoire, A., and Coauthors, 2013: The CNRM-CM5.1 global climate model: Description and basic evaluation. *Climate Dyn.*, **40**, 2091–2121, <https://doi.org/10.1007/s00382-011-1259-y>.
- Wall, C. J., and D. L. Hartmann, 2015: On the influence of poleward jet shift on shortwave cloud feedback in global climate models. *J. Adv. Model. Earth Syst.*, **7**, 2044–2059, <https://doi.org/10.1002/2015MS000520>.
- , —, and P.-L. Ma, 2017: Instantaneous linkages between clouds and large-scale meteorology over the Southern Ocean in observations and a climate model. *J. Climate*, **30**, 9455–9474, <https://doi.org/10.1175/JCLI-D-17-0156.1>.
- Walters, D., and Coauthors, 2019: The Met Office Unified Model global atmosphere 7.0/7.1 and JULES global land 7.0 configurations. *Geosci. Model Dev.*, **12**, 1909–1963, <https://doi.org/10.5194/gmd-12-1909-2019>.
- Watanabe, M., and Coauthors, 2010: Improved climate simulation by MIROC5: Mean states, variability, and climate sensitivity. *J. Climate*, **23**, 6312–6335, <https://doi.org/10.1175/2010JCLI3679.1>.
- Watt-Meyer, O., D. M. W. Frierson, and Q. Fu, 2019: Hemispheric asymmetry of tropical expansion under CO₂ forcing. *Geophys. Res. Lett.*, **46**, 9231–9240, <https://doi.org/10.1029/2019GL083695>.
- Wielicki, B. A., B. R. Barkstrom, and E. F. Harrison, R. B. Lee III, G. L. Smith, and J. E. Cooper, 1996: Clouds and the Earth's Radiant Energy System (CERES): An Earth observing system experiment. *Bull. Amer. Meteor. Soc.*, **77**, 853–868, [https://doi.org/10.1175/1520-0477\(1996\)077<0853:CATERE>2.0.CO;2](https://doi.org/10.1175/1520-0477(1996)077<0853:CATERE>2.0.CO;2).
- Wood, R., and C. S. Bretherton, 2006: On the relationship between stratiform low cloud cover and lower-tropospheric stability. *J. Climate*, **19**, 6425–6432, <https://doi.org/10.1175/JCLI3988.1>.
- Wu, P., M. Roberts, G. Martin, X. Chen, T. Zhou, and P. L. Vidale, 2019: The impact of horizontal atmospheric resolution in modelling air–sea heat fluxes. *Quart. J. Roy. Meteor. Soc.*, **145**, 3271–3283, <https://doi.org/10.1002/qj.3618>.
- Yettella, V., and J. E. Kay, 2017: How will precipitation change in extratropical cyclones as the planet warms? Insights from a large initial condition climate model ensemble. *Climate Dyn.*, **49**, 1765–1781, <https://doi.org/10.1007/s00382-016-3410-2>.
- Zelinka, M. D., S. A. Klein, and D. L. Hartmann, 2012a: Computing and partitioning cloud feedbacks using cloud property histograms. Part II: Attribution to changes in cloud amount, altitude, and optical depth. *J. Climate*, **25**, 3736–3754, <https://doi.org/10.1175/JCLI-D-11-00249.1>.
- , —, and —, 2012b: Computing and partitioning cloud feedbacks using cloud property histograms. Part I: Cloud radiative kernels. *J. Climate*, **25**, 3715–3735, <https://doi.org/10.1175/JCLI-D-11-00248.1>.
- , —, K. E. Taylor, T. Andrews, M. J. Webb, J. M. Gregory, and P. M. Forster, 2013: Contributions of different cloud types to feedbacks and rapid adjustments in CMIP5. *J. Climate*, **26**, 5007–5027, <https://doi.org/10.1175/JCLI-D-12-00555.1>.
- , C. Zhou, and S. A. Klein, 2016: Insights from a refined decomposition of cloud feedbacks. *Geophys. Res. Lett.*, **43**, 9259–9269, <https://doi.org/10.1002/2016GL069917>.
- , K. M. Grise, S. A. Klein, C. Zhou, A. M. DeAngelis, and M. W. Christensen, 2018: Drivers of the low-cloud response to poleward jet shifts in the North Pacific in observations and models. *J. Climate*, **31**, 7925–7947, <https://doi.org/10.1175/JCLI-D-18-0114.1>.
- , T. A. Myers, D. T. McCoy, S. Po-Chedley, P. M. Caldwell, P. Ceppi, S. A. Klein, and K. E. Taylor, 2020: Causes of higher climate sensitivity in CMIP6 models. *Geophys. Res. Lett.*, **47**, e2019GL085782, <https://doi.org/10.1029/2019GL085782>.
- Zhao, M., 2014: An investigation of the connections among convection, clouds, and climate sensitivity in a global climate model. *J. Climate*, **27**, 1845–1862, <https://doi.org/10.1175/JCLI-D-13-00145.1>.
- , and Coauthors, 2016: Uncertainty in model climate sensitivity traced to representations of cumulus precipitation microphysics. *J. Climate*, **29**, 543–560, <https://doi.org/10.1175/JCLI-D-15-0191.1>.